Recent advances in paleoclimatological studies of Arctic wedge- and pore-ice stable-water isotope records

Journal:	*Permafrost and Periglacial Processes*
Manuscript ID	PPP-19-0050.R2
Wiley - Manuscript type:	Special Issue Paper
Date Submitted by the Author:	21-Feb-2020

Complete List of Authors:	Porter, Trevor; University of Toronto - Mississauga Opel, Thomas; Alfred Wegener Institute Helmholtz Centre for Polar and Marine Research

Keywords:	ice wedges, pore ice, syngenetic permafrost, water isotopes, paleoclimatology

Recent advances in paleoclimatological studies of Arctic wedge- and pore-ice stable-water isotope records

Trevor J. Porter[1] & Thomas Opel[2,1]

[1]Department of Geography, University of Toronto – Mississauga, Mississauga, ON, L5L 1C6, Canada

[2]Alfred Wegener Institute, Helmholtz Centre for Polar and Marine Research, Telegrafenberg A45, 14473 Potsdam, Germany

Abstract

Late Pleistocene and Holocene ground ice are common throughout the Arctic. Some forms of relict ground ice preserve local meteoric water, and their stable oxygen- and hydrogen-isotope ratios can be used to reconstruct past air temperatures. In this paper, we review the formation and sampling of two forms of relict ground ice – wedge ice and pore ice – and recent (2010-2019) advances in paleoclimatological studies of ground-ice stable-isotope records in the Arctic. Recent advances are attributed to better chronological constraints and refined understandings of the systematics and seasonality of relict wedge ice and pore ice. A rich network of ice-wedge records has emerged, primarily from the Siberian Arctic, whereas pore-ice records are less common. The ice-wedge network depicts a robust pattern of late Pleistocene cooling, and remarkably similar temperature depressions during Marine Isotope Stages 3 and 2. Very high-resolution wedge- and pore-ice stable isotope chronologies have been established recently and used to reconstruct winter and summer climate histories and assess seasonal dependencies in insolation-forced climate. Reports of ancient (>125 ka BP) ground ice demonstrate the long-term persistence of relict ground ice, and its potential to expand our knowledge of Quaternary climate dynamics in the terrestrial Arctic.

Keywords: ice wedges; pore ice; syngenetic permafrost; water isotopes; paleoclimatology

1. Introduction

Permafrost not only responds to and drives climate change but provides an extraordinary archive preserving fossils and other natural indicators of environmental and climatic change. Sedimentation and freezing processes, temperature and hydroclimate, and the origin and evolution of permafrost landscapes over millennia can be reconstructed from a suite of natural indicators including: (i) sediments[1,2]; (ii) cryostructures[3]; (iii) molecular-, micro- and macro-fossils[4–7]; and (iv) geochemistry of relict ground ice[8,9]. This review focuses on the stable-isotope geochemistry of relict ground ice, specifically ice wedges and intra-sedimental pore ice, which offer the most promise for paleoclimate studies.

Precipitation $^{18}O/^{16}O$ and $^{2}H/^{1}H$ isotope ratios (hereafter $\delta^{18}O_{precip}$ and $\delta^{2}H_{precip}$) are sensitive proxies for air temperature at mid- to high-latitude regions[10] and can be preserved in relict ground ice for millennia. Ice wedges preserve cold-season precipitation that is integrated as meltwater that fills the cavity of thermal contraction cracks in spring[11]. As such, ice wedges offer a paleoclimate archive that specifically reflects winter conditions. . Structureless, interstitial pore ice originates from active-layer waters that froze *in situ*[3], and can integrate a blend of warm-season or annual precipitation depending on local climate and soil properties and, therefore, has a less specific seasonality than wedge ice. Nevertheless, pore-ice water-isotope ratios can be used to constrain past climate changes[12,13].

The association between precipitation isotopes and temperature[10] was first exploited by the glacial ice-core community for paleoclimate reconstruction more than a half-century ago[14], and has since been applied to different forms of relict ground ice[15,16]. Within the ice-core community, a relatively unified framework has emerged for quantitative climate reconstruction using stable-water isotopes[17]. Conversely, paleoclimate inferences from ground-ice stable-isotope records have generally been more qualitative (i.e., warmer vs. colder[18]. This tendency toward a more qualitative approach in the permafrost community may relate to challenges with the dating of relict ice, and proxy-climate uncertainties related to the precipitation-isotope system and the systematics of different forms of ground ice, all of which have some bearing on the fidelity of climate reconstructions.

Despite of these challenges, there is growing interest in the potential to use wedge- and pore-ice isotope records to constrain Quaternary climates in the unglaciated Arctic. This interest has increased the number of researchers participating in this field, and encouraged the generation of more quantitative datasets for use by the broader paleoclimate community in data-model comparisons[19] and their inclusion in paleoclimate databases[20,21]. Careful attention to these broader applications of ground-ice stable isotope records will ultimately increase the visibility of this field. In this paper, we review recent (2010-2019) advances in wedge- and pore-ice stable isotope studies in the Arctic (Fig. 1) and complement earlier reviews on the physics of ground ice formation[22], regional ice-wedge syntheses[23] and the scientific methods of ice-wedge paleoclimatology[11]. We start with a brief summary outlining the formation and preservation of meteoric waters in wedge ice and pore ice, and methodological topics including sampling and dating that have implications for the interpretation of relict ice records. Second, we present a meta-analysis of wedge-ice $\delta^{18}O$ data from 82 Northern Hemisphere sites (Fig. 1) and discuss the climatic origin of spatial patterns during the late Pleistocene and Holocene. Lastly, we review recent progress in paleoclimate knowledge gained from wedge- and pore-ice isotope records from a selection of studies located throughout the Arctic that highlight the diversity of insights these types of records offer the paleoclimate community.

FIGURE 1 HERE

Figure 1. Sites of recent studies of water isotopes in relict wedge ice (yellow circles) and pore ice (red squares); Russian sub-regions of W. Siberia (R1), Laptev Sea region (R2), Kolyma and Chukotka (R3) and central Yakutia (R4) are indicated; modelled permafrost zones[24] are indicated.

2. Systematics of relict wedge- and pore-ice formation

2.1 Wedge ice

Ice wedges form in polygonal patterns and grow due to the repetition of wintertime thermal contraction cracking of the ground, and the filling of frost cracks in spring[25]. Melt water from the winter snowpack is assumed to be the major constituent for filling frost cracks. It integrates the isotopic composition of winter precipitation and refreezes immediately in the crack to form an ice vein. According to Michel[26] this rapid freezing is a non-equilibrium freezing process with no or only insignificant isotopic fractionation. Minor contributions of hoar frost and dry snow, and detrital sediment and organic material washed into the crack by snowmelt may also contribute to ice veins.

Recent studies of ice crystallography, water isotopes and the composition and shape of gas bubbles, however, challenge this general assumption. St-Jean et al.[27] proposed that climate and site-specific conditions may determine the mode of ice wedge formation, with re-frozen snowmelt being more common in warm-wet environments, and hoar frost accretion/dry snow densification more common in cold-dry environments. They determined that the gas bubbles which form in ice wedges derived from hoar frost and dry snow are more spherical than the gas bubbles that form in a freezing liquid. Trace-gas concentrations of the bubbles also differ depending on the mode of ice formation[27]. These observations suggest that relatively simple physical measurements can be used to differentiate between genetic classes of wedge ice, which may hold value in refining paleoclimate interpretations of wedge-ice water-isotope data. Based on studies of both Pleistocene and Holocene ice wedges in Siberia, Boereboom et al.[28] emphasizes that crack-infilling material is a variable water-snow mix with a tendency toward higher proportions of snowmelt during warmer periods (e.g., Holocene), whereas Kim et al.[29] even exclude the participation of a liquid water phase in forming the studied late Pleistocene Marine Isotope Stage (MIS) 2 ice wedges in Central Yakutia.

Irrespective of the composition of the frost-crack infill material, it is evident that ice wedges originate from winter precipitation and, therefore, their stable-isotope composition represents a cold-season temperature signal.

2.2 Pore ice

In syngenetic permafrost, pore ice preserves precipitation or runoff that percolated through the active layer during past thaw seasons, froze at or near the permafrost table during the freeze-back period, and later became relict (i.e., fell below the permafrost table) following permafrost aggradation due to accumulation of surface materials. The pore waters that form pore ice may integrate (i) meltwater derived from snow and active-layer pore ice that formed during previous years, and (ii) warm-season precipitation that can penetrate the full depth of the active layer. The seasonality of precipitation in pore ice depends on local climatological factors such as mean air temperatures and monthly precipitation totals, as well as the thermal and hydraulic properties of the ground. For example, at a sloped peat plateau site in central Yukon, Porter et al.[13] found that *ca*. modern (last decade) pore ice integrated a multi-annual blend of primarily summer precipitation. They attributed this seasonality to (i) low permeability of the ice-rich peats to snowmelt at the start of the thaw season; (ii) efficient drainage of springtime precipitation as active layer runoff due to a higher saturated hydraulic conductivity at shallow thaw depths, (iii) a climatological bias with warm-season precipitation (mostly rain) accounting for roughly two-thirds of the annual precipitation budget, and (iv) a greater active layer thickness in the late summer that allows summer precipitation to reach the permafrost table where it has the potential to become relict pore ice. However, reports on the isotopic composition of pore ice from other northern sites indicate that pore ice can take on more of an annual seasonality[30], suggesting that site-specific conditions play an important role in determining the precipitation seasonality of relict pore ice.

In contrast to wedge ice, the relatively slow rates of freezing that occur in the active layer during the freeze-back causes pore water isotopes to fractionate between the liquid and solid phase, with a preference for heavy isotopologues ($^{1}H^{2}H^{16}O$ and $^{1}H_2{}^{18}O$) in the solid phase[31]. Assuming the range of experimentally constrained fractionation factors, the overall $\delta^{18}O$ enrichment of ice above water ($\varepsilon^{18}O_{i\text{-}w}$) is expected to be ~2.7-3.1‰ under equilibrium conditions (slow freezing rate and unimpeded molecular diffusion)[31]. However, $\varepsilon^{18}O_{i\text{-}w}$ values as low as 0.8-1.0% have been observed in natural active layers which suggests that non-equilibrium freezing conditions are common[13,32]. Since cryofractionation depends on rates of thermal and molecular diffusion, a constant $\varepsilon_{i\text{-}w}$ may be a reasonable assumption for any given sequence of syngenetic pore ice if the thermal and hydraulic properties of the paleo-active layer were constant. If a constant $\varepsilon_{i\text{-}w}$ is valid, as argued in some studies[13], it follows that stratigraphic isotope variations in syngenetic pore ice can be used as a first-order proxy for the isotopic composition of precipitation and climate. However, for permafrost sequences where paleo-active layer freezing conditions and $\varepsilon_{i\text{-}w}$ may have varied through time (e.g., due to a changing sedimentology and/or porosity), it may be more difficult to resolve the separate effects of changing $\varepsilon_{i\text{-}w}$ versus paleoclimate in the isotope stratigraphy of pore ice records.

3. Paleoclimate inferences from wedge- and pore-ice

Ice wedges have been widely used to reconstruct winter climate changes across Siberia on centennial to glacial/interglacial timescales[8,9,15], whereas paleoclimate estimates based on intra-sedimental pore ice has been investigated only in some pioneer studies[12,13,30]. Several quantitative transfer functions have been developed to estimate past air temperatures based on wedge- and pore-ice isotope ratios, using either the relation between regional climate and isotope data from modern ice wedges or modern precipitation (see Opel et al.[11] for a compilation and discussion of transfer functions). More commonly, the stable-isotope variations of relict ice wedges are used for qualitative winter temperature inferences[18].

The accuracy of paleotemperature estimates based on isotope trends in relict ground ice depends on the assumptions that the precipitation seasonality of relict ice and the relation between precipitation-isotope ratios and air temperatures were constant. While this is often assumed for recent timescales, its validity over glacial-interglacial timescales has been debated at length[33]. Under a constant set of ocean-atmosphere boundary conditions, real or apparent changes in precipitation seasonality and temperature-isotope sensitivity are not expected. However, over glacial timescales when the land-ocean configuration (e.g., sea level, ice sheet topography) was different from today with possible differences in moisture source and trajectory of moist air parcels, there is greater potential for non-temperature related effects in the isotope record. Isotope-enabled General Circulation Models provide opportunities to evaluate the physical processes driving precipitation isotopes and potential changes in temperature sensitivity in response to changing ocean-atmosphere boundary conditions[34].

Finally, differences in global ocean volume may also significantly influence ground ice-isotope records. During the Pleistocene cold stages, the $\delta^{18}O$ and $\delta^{2}H$ of the global ocean was more positive than today due to the increased storage of isotopically depleted water on land in polar ice sheets[35]. Quantitative temperature reconstructions based on ice-core $\delta^{18}O$ records typically correct for changes in seawater[17]. This same approach has been applied in a limited number of pore-ice[13] and wedge-ice[30] studies. However, as the isotopic composition of seawater can vary dramatically over relatively short timescales (e.g., MIS 2-1 transition), explicit seawater corrections to ground-ice and ice-core isotope records require good chronological control to determine an appropriate correction. Seawater corrections are crucial for quantitative paleoclimate estimates. Further, comparison of $\delta^{18}O$ values from relict ice of different ages for qualitative temperature inferences would also benefit from standardizing isotope data to a constant ocean.

4. Sampling and dating of relict ground ice

As for all paleoclimate archives, precise dating and chronology development is crucial for meaningful paleoclimate reconstruction. Furthermore, criteria for inclusion of paleoclimate records in multi-proxy databases are often tied to chronology characteristics[36], so recognition of ground-ice studies as a subdiscipline of quantitative paleoclimatology will require careful attention to chronological standards set by the broader community. The type of chronology that can be developed for wedge and pore ice depends on the type of samples collected. In general, ice wedges can be dated indirectly by dating the host sediments or dated directly by dating the ice itself, whereas pore ice can only be dated indirectly from the host sediments.

Ice-wedge sampling strategies have evolved over the last two decades. Early studies commonly used only a few samples per ice wedge taken by ice screw, axe or gas-powered drill, while in recent years chainsaws have become the standard tool for fast and defined sampling (Fig. 2A). To account for the growth pattern of ice wedges in both horizontal and vertical dimensions mainly two sampling schemes have been used: either cutting ice blocks (Fig. 2B-C) or defined sampling resolution by cutting thin slices (Fig. 2D). Preferentially large blocks are collected, which are subject to later handling and subsampling in a freezing lab to ensure the highest quality of samples and reduced risk of contamination, and possible identification of individual ice veins for sub-sampling (Fig 2E). Ice wedges are mostly sampled in exposures at coastal, lake or river cliffs or the headwalls of retrogressive thaw slumps. Ice wedge sampling has also been possible in tunnels dug into the permafrost[18,37–39].

FIGURE 2 HERE

Figure 2. Ice-wedge and pore-ice sampling. (A) Ice-wedge sampling by chainsaw; (B,C) block cuts from an ice wedge; (D) slice cut from an ice wedge; (E) internal foliation of an ice wedge with visible ice veins and sediment and organic inclusions; (F) pore-ice sampling by lateral coring of a permafrost exposure using a hand-held drill; (G) pore-ice sampling by vertical coring into permafrost using a gas-powered drill; and (H) recovering the permafrost core from the 'core catcher'.

Drilling boreholes horizontally (Fig. 2F) or vertically (Fig. 2G-H) into sediment-rich permafrost is the preferred approach for pore-ice studies. Vertical coring includes the time component and is the easiest sampling approach, but it only yields point information which does not necessarily account for complex three-dimensional cryostratigraphy of ice-rich permafrost. Hence, it may be accompanied by discrete sampling of permafrost exposures.

Age determination of host sediments has been achieved mostly by radiocarbon dating of associated plant macro-remains or bulk organics[13,40,41], but also by optically stimulated luminescence (OSL) of quartz grains[39], infrared stimulated luminescence (IRSL) of feldspar grains[9], peat radioisotope disequilibrium[42,43], geochemical fingerprinting or fission-track dating of glass shards in tephra beds[44], and paleomagnetic dating[45]. For indirect dating of ground ice one has to keep in mind that relict ice wedges and pore ice are younger than the host sediment at the same level. For ice wedges this is due to the downward directed frost crack filling, and for pore ice this is due to the mobility of liquid water in the unfrozen active layer prior to freezing. In both cases the ground ice is hosted in sediments that were deposited sometime before the ice formed. The age offset between the relict ice and the host sediments depends on the cracking depth for ice wedges, or maximum penetration depth of the pore waters in the active layer (i.e., the maximum active layer thickness) for pore ice, as well as the permafrost aggradation rate in syngenetic permafrost systems.

The standard approach for direct dating of ice wedges is AMS radiocarbon dating. For most late Pleistocene and Holocene studies plant macrofossils are used[9,18,46]. In recent years, radiocarbon dating of dissolved organic carbon ($DO^{14}C$)[38,47] and $^{14}CO_2$ of air bubbles in the wedge ice[29,38] has been successfully applied.

For a late Pleistocene ice wedge in Alaska, Lachniet et al.[38] showed that $DO^{14}C$ and $^{14}CO_2$ ages are younger than the fine-dispersed particulate organic matter and plant-macro remains and suggested that the first are geologically more reasonable. The temporal limit of the radiocarbon dating method precludes dating of ground ice older than ~50,000 years (middle-MIS 3). An independent direct dating approach using the ratio of cosmogenic chlorine-36 (^{36}Cl) to chloride (Cl^-) in wedge ice reaches back to the middle to late Pleistocene[48], but requires further proof and refinement.

Further method development and refinement to date old ground ice is needed as it becomes more evident that, despite its susceptibility to climate warming, ice-rich permafrost can be very persistent and survive even several interglacials. Relict ice wedges from Yukon (740,000 ± 60,000 yr BP)[44] and Bol'shoy Lyakhovsky Island (~ 200,000 yr BP)[43] predate the oldest ice recovered from the base of the Greenland ice sheet[49] and possibly represent the oldest ice in the Northern Hemisphere. Reliable dating of such ancient permafrost is a precondition to shed light on the controls of such remarkable permafrost persistence.

The temporal resolution of most relict wedge-ice records is relatively coarse, for example, binned into stratigraphic units or marine isotope stages or sub-stages (e.g., late MIS 3 or 'full glacial' MIS 2). However, there are examples of wedge-ice time-series with exceptionally high temporal-resolution chronologies (e.g., decadal to centennial). Basically two approaches have been successfully utilized to generate these time-series from ice wedges: age-distance interpolation between radiocarbon dated samples within an ice-wedge profile[18] and combining paired age-isotope information into a composite record[8,50]. However, application of statistical age-distance models for high-resolution ice-wedge chronologies is relatively uncommon as the underlying assumptions of such models (i.e., continuous growth rate and absence of cross-cutting ice veins) are difficult to verify or are often violated on the basis of ^{14}C-age reversals[38,50].

Indirect dating of relict pore ice in a syngenetic permafrost sequence has been approximated in two ways. First, stratigraphic association with dated macrofossils[16] or with geochemically verified tephra of known age[51] in the host sediments gives a maximum age constraint on the pore ice. Second, age interpolation using an age-depth model may be constrained by ^{14}C-dated macrofossils and other chronological tie-points (e.g., tephra) in the permafrost sequence[13]. This method assumes that the formation of relict pore ice and paleosurface (and paleo-permafrost) aggradation occurred simultaneously, and that the formation depth of relict pore ice (i.e., maximum thaw depth) did not vary much through time[13]. The latter assumption has implications for the interpolated age of the pore ice. For example, given a constant maximum active layer thickness of 60 cm, the age of any relict pore-ice sample in the permafrost sequence will be equal to the age of sediment found 60 cm above, which can be referenced from the sediment (paleosurface) age-depth model. The youngest 'relict' pore ice, with an approximate age of ca. present day, is found in the uppermost layer of permafrost.

5. Major paleoclimate results since 2010

5.1 Spatial and temporal patterns of ice-wedge $\delta^{18}O$ data

For a meta-analysis, we have summarized mean ice-wedge $\delta^{18}O$ data across the northern high latitudes for several periods: MIS 3 (57-29 cal ka BP), MIS 2 (29-11.7 cal ka BP), Holocene (last 11.7 cal ka BP) and modern (last several decades) in order to examine broad spatial and temporal patterns (Fig. 3). This extends earlier work[23,52,53] mainly by including data from Alaska and Canada. In total, we considered ice-wedge $\delta^{18}O$ records from 82 study sites (Table S1). Although the meta-analysis focuses on the MIS 3-1 and present-day intervals, a few rare examples of older (MIS 7 to 4) ice-wedge $\delta^{18}O$ records are discussed in sections 5.2.2 and 5.2.4. We are aware that (i) climate was not constant during all four intervals, (ii) mean $\delta^{18}O$ data of the ice wedges may represent only part of these periods, and (iii) dating uncertainties exist for the ice wedges and host sediments, respectively. Even though these issues add a certain degree of uncertainty, robust spatial and temporal patterns are evident in the ice-wedge $\delta^{18}O$ data from which general conclusions can be drawn.

FIGURE 3 HERE

Figure 3. Average wedge-ice $\delta^{18}O$ values dating to (a) modern, (b) Holocene, (c) MIS 2 and (d) MIS 3 from studies since 2010 (see Table S1 for data and sources); Russian sub-regions of W. Siberia (R1), Laptev Sea region (R2), Kolyma and Chukotka (R3) and central Yakutia (R4) are indicated.

$\delta^{18}O$ data of *ca.* modern ice wedges (Fig. 3a), i.e. those which formed in the last several decades according to stratigraphic interpretation or post-bomb isotope data (e.g., ^{14}C or ^{3}H), are most enriched and in most cases exceed the mean Holocene $\delta^{18}O$ values (Fig. 3b) by several permil. This reflects recent Arctic warming which is particularly evident in the extended winter season as also shown in temperature reconstructions based on ice wedges (Fig. 4a). Holocene wedge-ice $\delta^{18}O$ mean values are clearly enriched over late Pleistocene wedge-ice $\delta^{18}O$ mean values of MIS 3 (Fig. 3d) and MIS 2 (Fig. 3c) which reflect a colder mean winter climate during past stadials and interstadials in comparison to the present interglacial. MIS 3 and MIS 2 are characterized by similar wedge-ice $\delta^{18}O$ values, with only a few surprising exceptions for sites that show lower $\delta^{18}O$ values during MIS 3 than MIS 2. In the circum-Arctic, the MIS 3 interstadial is often assumed to represent a milder but also more variable climate than the full glacial conditions of MIS 2 that culminated in the Last Glacial Maximum (LGM) at ~21 ka BP[19]. This apparent discrepancy may be due in part to the winter seasonality of ice wedges and/or to the time integrated in MIS 3 and MIS 2 ice wedges. For example, some MIS 2 ice wedges capture the deglacial period[18], but almost certainly do not represent the extreme cold or LGM conditions of MIS 2. Further, some areas show a general absence of MIS 2 ice wedges dating to the full glacial[30,47], which may indicate conditions that inhibited the development (e.g., thicker snow[16]) or preservation of ice wedges. A lack of MIS 2 ice wedges is also observed in parts of the Russian Arctic, where MIS 2 full glacial permafrost deposits (i.e. Sartan Yedoma Ice Complex) may have formed only in specific environments such as river valleys[40]. MIS 2 ice wedges from such Ice Complex deposits on

Bol'shoy Lyakhovsky Island, for example, show extremely depleted $\delta^{18}O$ values as low as –37‰ (or 6‰ lower than MIS 3 ice wedges), while MIS 2 ice wedges from other sites in the Laptev Sea region do not show more depleted $\delta^{18}O$ values compared to MIS 3[40].

Spatial patterns in ice-wedge $\delta^{18}O$ are evident in all time slices from modern to MIS 3 (Fig. 3) and are generally consistent with those of modern winter precipitation isotopes[54]. Coastal ice wedges are more enriched in $\delta^{18}O$ compared to more continental ice wedges, likely reflecting the smaller distance to the moisture source. A remarkable feature is the zonal $\delta^{18}O$ trend across the coastal Russian Arctic with $\delta^{18}O$ values decreasing from west to east. This pattern likely reflects a dominance of westerly moisture transport from the North Atlantic and Rayleigh distillation along a west-east temperature gradient that was a constant feature of the last ~60 kyr, independent of climate and ice-sheet configuration. Study sites in Chukotka in easternmost Russia show more enriched values and reflect mainly Pacific moisture sources[55].

This spatial analysis is somewhat limited by the fact that most ice-wedge study sites are located in the Russian Arctic and/or along the coast, whereas the North American Arctic sites are too sparsely distributed to resolve regional spatial trends.

5.2 Major paleoclimate results from Russian Arctic sites

Studies of relict ground ice for paleoenvironmental reconstruction in the Russian high latitudes date back more than three decades[15] and have led to a remarkable collection of data. . In the following sections we briefly review major progress over the last 10 years in 4 main regions (West Siberia, Laptev Sea region, Kolyma region and Chukotka) and Interior Yakutia.

5.2.1 West Siberia

Only a few studies exist for West Siberia. Based on syngenetic ice wedges of MIS 2 and Holocene age at three sites at the eastern coast of the Yenisei Bay (Western Taymyr Peninsula), Streletskaya et al.[56] demonstrate that this part of the Taymyr Peninsula was not glaciated during the LGM. The authors infer warming since the MIS 2, with mean $\delta^{18}O$ values of about –26‰ during MIS 2 increasing to Holocene mean $\delta^{18}O$ values of –20.5‰. Modern ice wedges are even more enriched above the Holocene wedges by a similar amount, with a $\delta^{18}O$ value of about –16.5‰. For the MIS 2 ice wedges, Streletskaya et al.[56] estimated a mean January temperature of around –40°C, which is 12-15°C colder than at present. The increase in $\delta^{18}O$ is accompanied by an increase in d_{excess} ($\delta^2H - 8\times\delta^{18}O$) from mean values of ~8-9‰ to ~11-13‰. Similar $\delta^{18}O$ values for Holocene and modern ice wedges are observed on the Southern Yamal Peninsula[57].

Given its proximity to the western boundary of the permafrost zone and to the Barents and Kara seas, which both are particularly affected by modern and likely also past Arctic climate and sea-ice changes, West Siberia may be a key region for future detailed ice-wedge paleoclimate studies.

5.2.2 Laptev Sea region

Over the last decades the Laptev Sea region has been one of the main study regions for relict permafrost in the Russian Arctic. The late Pleistocene Yedoma Ice Complex of MIS 3 to 2 age and its degradation forms (i.e., thermokarst basins) are major landform elements in the coastal lowlands of the region. However, at the Dmitry Laptev Strait two older Ice Complex units have been studied, dating to MIS 7[43] and MIS 5[42].

Three Ice Complex units share similar mean wedge-ice $\delta^{18}O$ values: MIS 7 (–32‰), MIS 5 (–33‰) and MIS 3 (–31‰) indicating comparable winter temperatures during the MIS 7 interglacial and the MIS 5 and MIS 3 interstadials. In contrast, the MIS 2 Ice Complex is characterized by a mean wedge-ice $\delta^{18}O$ value of –37‰, indicating significantly colder mean winter temperatures during the stadial towards the LGM, an unprecedented pattern for the Russian Arctic[43]. It should be noted that the MIS 5 Buchchagy Ice Complex does not capture the globally warm last interglacial period, i.e. MIS 5e[42]. The thermokarst-lake and thermokarst-basin palustrine deposits of the Krest Yuryakh Suite (formerly attributed to MIS 5e) are most likely degradation forms of the Buchchagy Ice Complex. They have been IRSL-dated to 102.4 ± 9.7 ka[9], placing them within the MIS 5d stadial. Further dating and isotopic studies are necessary to solve this puzzle of Northeast Siberian climate and landscape dynamics.

Interestingly, the mean d_{excess} values are quite similar across all four Ice Complex units, indicating similar atmospheric moisture generation and transport patterns in winter[43]. Cold stage conditions similar to the MIS 2 are reflected by mean ice-wedge $\delta^{18}O$ values of –36‰ for MIS 4 ice wedges preserved in floodplain deposits.

Much warmer winter temperatures can be inferred from Holocene (mean $\delta^{18}O$ of –25‰) and in particular modern (mean $\delta^{18}O$ values of –20.5‰) ice wedges, clearly reflecting the interglacial Holocene and recent Arctic warming[9]. Winter temperature trends at higher (i.e. centennial) resolution have recently been obtained from Holocene ice wedges preserved in river terraces and on top of the Yedoma Ice Complex in the Lena Delta[8]. A composite wedge-ice $\delta^{18}O$ record from the Lena Delta[8], based on paired ^{14}C ages and $\delta^{18}O$ data of 42 ice-wedge samples, and additionally modern ice wedges, shows a long-term $\delta^{18}O$ increase ($\Delta\delta^{18}O$ = +0.45‰·ka^{-1}) until AD 1850. It indicates a warming trend in winter (December to May) that began as early as the mid-Holocene, which has been followed by unprecedented warming in the last ~150 years (Fig. 4a). This first evidence of a Holocene winter warming trend differs from long-term cooling seen in most other high-latitude temperature proxies that are biased towards the summer and are driven by declining summer insolation. In contrast, the cold-season warming may be largely explained by long-term increases in cold-season (November to April) insolation (Fig. 4b) and greenhouse gas forcing. The Holocene winter warming is corroborated by paleoclimate model simulations[8]. While the Lena Delta record does not show a significant trend over the last two millennia, except for the unprecedented recent warming, a second record from a drained thermokarst basin at the Oyogos Yar coast[50] shows a pronounced warming trend over this period and the modern era ($\Delta\delta^{18}O$ = +1.5‰·ka^{-1}) (Fig. 4a).The warming towards present conditions is detectable in the high-resolution stable-isotope profiles from all three ice wedges studied at this site.

FIGURE 4 HERE

Figure 4. Holocene paleoclimate reconstructions and relict ground-ice water-isotope records. (a) Multi-site stacked wedge-ice $\delta^{18}O$ record from the Lena Delta[8] (black dashed line) and a single-site stacked wedge-ice $\delta^{18}O$ record from the Oyogos Yar coast[50] (red dashed line); (b) insolation change relative to modern during the warm-season (Jun-Sep) and cold-season (Nov-Apr) after Laskar et al.[58]; (c) pore-ice $\delta^{2}H$ record from DHP174 site in central Yukon[13]; (d) Northern Hemisphere multi-proxy temperature reconstruction[59].

5.2.3 Kolyma region and Chukotka

The lower reaches of the Kolyma River have been an important region for ice-wedge paleoclimate research[15]. At different sites along the roughly 10 km-long exposure of the Duvanny Yar Ice Complex key site (MIS 3 to MIS 2), vertical $\delta^{18}O$ profiles vary between about –33 and –30‰, partly in a cyclic pattern and slightly decreasing upwards[2]. Vasil'chuk[60] interpreted some of the spiky maxima in the Duvanny Yar and other regional ice-wedge sites as possible Dansgaard-Oeschger events, decadal- to multi-decadal climate oscillations of the North Atlantic sector during MIS 3, as observed in Greenland ice cores[61]. However, the relatively coarse dating and dating uncertainties of the Duvanny Yar isotope stratigraphy makes attribution to any specific Dansgaard-Oeschger event difficult. If Dansgaard-Oeschger events are truly represented in the Kolyma region this would have major implications for our understanding of the role the North Atlantic Thermohaline Circulation plays in regulating broader scale climate variability across the Arctic. At the Plakhinskii Yar

Ice Complex site, a vertical ice-wedge profile covering the latest MIS 3 and full MIS 2 (~30-12 ka) reveals a larger $\delta^{18}O$ variability ranging from –34.7 to –30‰[62]. The coldest period in the record (30-28 ka) is attributed to Heinrich Stadial 3. Another cold period around 18-16 ka reaches similarly depleted values, followed by a warming ($\delta^{18}O$ values between –31 and –30‰). In contrast to these sites, the wedge-ice $\delta^{18}O$ profile of the Stanchikovsky Yar Ice Complex suggests stable climate conditions between 35 and 25 ka[63]. The Ice Complex at Ayon Island in Kolyma Bay shows rather variable wedge-ice $\delta^{18}O$ values between –34 and –29‰ for the period 30 to 10 ka with lower values in the first half of the record, whereas Holocene ice wedges reflect much higher temperatures with a mean $\delta^{18}O$ value of –21.6‰[64].

Distinctly more enriched $\delta^{18}O$ values ranging from –29 to –26‰ are observed in a vertical ice wedge profile dated to 42 to 27 ka at the Ledovy Obrykh site in the Mayn River valley in Chukotka[65]. An upwardly decreasing trend during the MIS 3 to 2 transition was interpreted as a cooling trend. Again, Holocene wedge ice at this site is substantially enriched in $\delta^{18}O$ and yields a mean value of –20‰.

The East Chukotka Peninsula receives between 40 and 60% of its precipitation from the Northern Pacific Ocean[55]. Stable isotopes of early and middle Holocene ice wedges at three sites on the East Chukotka Peninsula[55] clearly reflect this proximity to the main moisture source. They are distinctly enriched compared to more continental sites in Chukotka and most other study sites in the Russian High Latitudes, and similar to those from West Siberia. Mean $\delta^{18}O$ values per wedge vary between –18.5 ‰ and –14‰. Mean d_{excess} values are also similar to West Siberia, ranging between 8 and 13‰. Modern ice wedges show more enriched $\delta^{18}O$ values (–13‰) and lower d_{excess} (6‰), reflecting modern warming and associated changes in moisture generation and transport dynamics.

5.2.4 Interior Yakutia

Interior parts of Yakutia are understudied compared to the coastal sites of the Russian Arctic, but there are new ice-wedge stable-isotope data and insights on past winter climate in this highly continental region from the Batagay megaslump in the Yana Highlands.

Vasil'chuk et al.[66] and Opel et al.[52] revealed consistent mean $\delta^{18}O$ values of around –35‰ for several ice wedges of the upper ice complex unit of the slump headwall attributed to the MIS 3 interstadial. Such depleted values have not been observed in other MIS 3 deposits in all of Siberia[52,66], which suggests this region then had, as it does today, an extreme continental climate (Fig. 3). Additionally, the mean d_{excess} values of the Batagay and other Central Yakutian sites exhibit the highest mean values (≥ 8‰) in comparison to other MIS 3 ice wedges across Siberia[52].

While no Holocene ice wedges have been found in the Batagay megaslump, a late Holocene ice wedge from nearby at the Adycha River also exhibits more depleted mean $\delta^{18}O$ values (–29‰) compared to other study sites across Siberia indicating the high continentality but similar d_{excess} values[52]. How exactly the spatial d_{excess} pattern is influenced by the degree of continentality remains a topic for future studies. Interestingly, the $\delta^{18}O$ difference between MIS 3 and the Holocene (6‰) is about the same as for the Dmitry Laptev Strait.

The age of the lower ice complex exposed in the Batagay megaslump is not yet well known. Luminescence ages of 142.8 ± 25.3 kyr and >123.2 kyr (OSL) and 210.0 ± 23.0 kyr (IRSL) for the discordantly overlying lower sand unit suggest that the age of the Lower Ice Complex is MIS 6 or older. It could represent the oldest wedge ice ever analyzed for stable isotopes. Notably, it is clear that this ice complex has survived at least 2 Interglacials (in MIS 5 and Holocene), which demonstrates the local persistence of permafrost under suitable conditions. The mean wedge-ice $\delta^{18}O$ value of –33‰ reflects a cold winter climate that is comparable, but not as cold as MIS 3[52].

5.3 Major paleoclimate results from North American Arctic sites

Compared to the Russian Arctic, the western North American Arctic has seen less activity in the study of relict ground-ice stable-isotopes as a paleoclimate proxy, although there is a long history of studies in this region where relict ice stable-isotope records have been used for other purposes such as age and genetic classification of ground ice[67,68]. Nevertheless, there are several relevant studies from the last ten years that have contributed to advances in knowledge of Arctic paleoclimate, mainly from the Yukon-Alaska Arctic coast and continental Yukon-Alaska.

5.3.1 Yukon and Alaskan Arctic coasts

Studies of relict ice wedges from the Yukon and Alaskan Arctic coasts offer cold-season paleoclimate insights primarily dating to the deglacial phase of MIS 2 and the Holocene.

Discrete sampling of ice wedges has been reported from several localities along the Canadian western Arctic coast where upper late Pleistocene and Holocene permafrost is exposed. At Herschel Island, which is one of the few Canadian sites where both MIS 2 and Holocene ice wedges are reported, Fritz et al.[69] found a roughly 7‰ increase in mean $\delta^{18}O$ from -29‰ (Wisconsinan deglacial, ~16 ka BP) to -22‰ (mid-Holocene) which the authors interpret as due to winter warming. This was validated by a similar mean Holocene value of -23‰ for ice wedges at Komakuk Beach ~30 km west of Herschel Island[69] and King Point, ~70 km southwest of Herschel Island[70]. The chronology of the Herschel Island ice wedges, however, is only loosely constrained by the dating of the associated sedimentary units, and so these $\delta^{18}O$ data are only considered as broadly representative of the MIS 2 deglacial and Holocene periods.

On the north coast of Alaska near Barrow (Utqiaġvik), Meyer et al.[18] reported a ~3,000 year-long continuous record of wedge-ice $\delta^{18}O$ and d_{excess} from the Barrow Ice Wedge System (BIWS). Importantly, this record provides the only known sequence of wedge-ice $\delta^{18}O$

capturing the deglacial transition from the Bølling-Allerød (BA) interstadial to Younger Dryas (YD) stadial conditions ~12.9 ka BP, and the subsequent onset of Preboreal warming at ~11.5 ka BP. A second novel aspect of this record is a companion pollen dataset developed from the host sediments[37] which allowed the authors to resolve the local paleoecology and summer temperature history, in addition to the winter temperature history, which demonstrates the potential to develop multi-proxy and seasonally holistic records of paleoenvironmental change from ice wedge-bearing permafrost units.

FIGURE 5 HERE

Figure 5. Water isotope and phytoplankton-derived methanesulfonate ion (MS^-) records dating to the Younger Dryas transition from the Barrow Ice Wedge System (BIWS) and NGRIP ice core. (a, b) $\delta^{18}O$ and d_{excess} records from BIWS[18] (red circles) and NGRIP[71] (black line). (c) MS^- ion concentration from BIWS[72] (red circles).

The BIWS $\delta^{18}O$ record documents a ~5‰ decrease (from -22‰ to -27‰) at the BA-YD transition ~12.8 ka BP, which is similar to a ~6‰ decrease in the NGRIP (Greenland) ice core $\delta^{18}O$ record since ~14.5 ka BP (Fig. 5a). The authors noted that this change in the BIWS record likely represents extreme cooling of local winter conditions, although they did not quantify the magnitude of cooling. After 11.5 ka, the formal limit of the YD, the BIWS and NGRIP records both show a rebound to mean $\delta^{18}O$ values that were more typical during the BA interstadial (Fig. 5a). The coherence of the BIWS and NGRIP records has major climatological implications, and suggests the Arctic system was tightly coupled at broad geographic scales during deglacial times, a conclusion that has since been extended to the North Pacific[73]. Meyer et al.[18] also observed coherent changes in the BIWS and NGRIP d_{excess} records (Fig. 5b), implying major changes in moisture source evaporative boundary conditions, but for the BIWS specifically this change was linked to flooding of the Alaskan continental shelf due to deglacial sea level rise. Last, another notable finding from the BIWS is the indication from the companion pollen record that YD summers in that area were not much colder than today[37], implying important seasonality differences in the expression of the YD climate event on the Alaskan north coast. This finding of relatively warm summers during a period that is generally thought of as extremely cold is curious, but also finds some support from an independent study by Iizuka et al.[72] that inferred relatively low sea ice concentrations just offshore from the BIWS site during the early YD.

Iizuka et al.[72] revisited the BIWS and analyzed the wedge ice for marine-derived aerosols, often applied in glacier ice-core studies for reconstructing sea ice concentrations. They observed high methanesulfonate ion (MS^-) concentrations during the early and coldest YD periods, indicating a high marine productivity and, therefore, nearshore open water conditions during the summer in the Beaufort Sea near Barrow, Alaska (Fig. 5c). This novel application of the MS^- proxy in ice wedges demonstrates a potentially new direction that can fill gaps in our knowledge of paleo-sea ice conditions in Arctic coastal settings.

5.3.2 Continental Alaska and Yukon

Recent studies in continental Alaska and Yukon that have used ground ice stable isotope ratios for paleoclimate reconstruction are mostly based on wedge ice[30,38,74], but also include rare examples where syngenetic pore ice has been used[13,30].

At the Fox Creek (CRREL) permafrost tunnel near Fairbanks, Alaska, Lachniet et al.[38] reported $\delta^{18}O$ values from a single ~1.2 m wide ice wedge, which likely formed during the full glacial between ca. 28-22 cal ka BP according to modeled $^{14}CO_2$ ages of air bubbles in the ice. Lachniet et al.[74] observed a mean $\delta^{18}O$ value of -27.2‰ for the most depleted wedge ice, which they suggested may reflect the coldest conditions of the LGM. Lachniet et al.[74] noted that the LGM mean value is depleted by 5.4‰ compared to nearby Holocene ice wedges ($\delta^{18}O$ = –21.8‰)[75], which they equated to a temperature depression of ~17 ± 3°C colder than modern assuming a winter $\Delta\delta^{18}O_{precip}$-temperature sensitivity of 0.31‰·°C^{-1}.

From the Klondike area of central Yukon, Porter et al.[30] reported wedge-ice $\delta^{18}O$ values of –29.3‰ for the late MIS 3 (*ca.* 31.9-30.2 cal. ka BP) and –24.5‰ for the late Holocene (*ca.* 0-500 year BP), respectively. Based on the 4.8‰ mean difference between the MIS 3 and late Holocene wedge-ice $\delta^{18}O$ values (5.5‰ after standardizing for $\delta^{18}O_{seawater}$) and an assumed $\delta^{18}O_{precip}$-ΔT sensitivity of 0.41‰·°C^{-1}, they estimated that MIS 3 winters in the Klondike were ~13 ± 3°C colder than modern. This value is similar to the ~17 ± 3°C temperature depression estimated by Lachniet et al.[74] from LGM wedge ice in central Alaska, implying that extremely cold winter climates prevailed across Eastern Beringia during MIS 3 and 2. Pore ice from the same Klondike deposits, thought to integrate annual precipitation, showed mean $\delta^{18}O$ values of –28.0‰ and –22.7‰ for MIS 3 and MIS 1, respectively[30]. Based on the 5.3‰ offset (6.0‰ after standardizing for $\delta^{18}O_{seawater}$) Porter et al.[30] estimated mean annual temperatures during MIS 3 were depressed by up to ~15 ± 3°C compared to the Holocene, which is similar to the MIS 3 winter temperature depression inferred based on wedge ice. However, the authors cautioned that paleotemperature estimates based on isotope ratios of pore ice containing an annual mixture of meteoric water are inevitably more sensitive to changes in the precipitation seasonality than relict ice with a more narrowly constrained seasonality (e.g., ice wedges).

Finally, a study by Porter et al.[13] reported the first full-Holocene, quantitative summer-temperature reconstruction based on pore-ice δ^2H (Fig. 4c) from a 5.3 m core of syngenetic permafrost below a soligenous peatland site (DHP174 site) in central Yukon. Porter et al. argued that the δ^2H variable provides a better estimate of paleotemperature compared to $\delta^{18}O$ since the deuterium-rich isotopologue of water (i.e., HDO) is less sensitive than $H_2{}^{18}O$ to evaporation-related kinetic effects that may occur at the oceanic moisture source, which can otherwise distort the paleoclimate signal recorded in pore ice[13]. The DHP174 pore-ice record integrates mainly summer precipitation (discussed in Section 2.2). After correcting for long-term seawater changes, the DHP174 pore-ice δ^2H record was used to reconstruct a 13.6 ka-long summer temperature history assuming the $\Delta\delta^2H_{precip}$-temperature sensitivity of ~1.6‰·°C^{-1}. The reconstruction shows deglacial warming since 13.6 ka BP and reaching a

Thermal Maximum at 7.6-6.6 ka BP when summers were ~0.3°C warmer than the Holocene mean. A subsequent 6 ka-long cooling trend (-0.16°C per ka) was abruptly reversed at the start of the Industrial Era (~200 years ago) when temperatures began to rise, culminating in the warmest summer climate at present day and exceeding the Thermal Maximum by ~2°C. General trends in the early, middle and late Holocene portions of the DHP174 pore-ice δ^2H record are consistent with a multi-proxy composite temperature reconstruction representing the northern extratropical latitudes[59] (Fig. 4d). Furthermore, apparent coupling between the reconstructed summer temperatures in Yukon and summer (June-Sept.) insolation at 65°N (Fig. 4b) implies solar forcing played a major role in driving regional Holocene climate trends.

6. Conclusions and outlook

The application of relict ground ice-stable isotopes for paleoclimate studies has advanced significantly in recent years and led to important insights on Quaternary climate dynamics across the Siberian Arctic and W. North American Arctic. Recent progress is clearly related to advances in ground-ice dating methods, development of high temporal-resolution (e.g., centennial to decadal) composite ground-ice isotope time-series and refined frameworks used to interpret these records, but ultimately driven by demand for paleoclimate data from the broader research community to constrain past (and potentially future) Arctic change.

Future studies are needed to harness the momentum and growing interest in relict ground-ice stable isotope paleoclimatology, and we recommend the following research directions:

- continued advancement of the scientific methods of ground-ice studies, including dating and chronology development;
- continued studies on the isotope systematics of relict ground-ice stable isotopes to enable refined interpretations and quantitative paleoclimate estimates[11];
- investigate the paleoclimate value of stable water isotopes in other forms of relict ground ice such as segregated ice lenses and buried ice (e.g., icings[51] and perennial snowbanks[76]);

- close spatial gaps, particularly in the Western Arctic where the concentration of relict ground-ice isotope records is low compared to the Russian Arctic (see Fig. 3);
- close temporal gaps in regions with available ground ice and reduced data density during MIS 2 and MIS 3 in comparison to the Holocene (see Figs. 3c-d);
- continued focus on climate patterns and periods of significance to the paleoclimate community such as the Common Era (last 2,000 years), the Holocene Thermal Maximum, LGM, and extreme variability such as Dansgaard-Oeschger events and the Younger Dryas, in order to assess the magnitude and dynamics of these climate phenomena across the pan-Arctic;
- further exploration and development of stable water-isotope records from ancient (e.g., middle Pleistocene) ground ice[52] which offer rare glimpses of the Arctic climate system during intervals that are simply not captured by any other terrestrial archive in the Northern Hemisphere;
- develop a suitable repository for ground-ice stable isotope records that conforms to the data and metadata standards expected by the broader paleoclimate and climate-modeling communities;
- validate novel proxies such as sea-spray aerosols preserved in ice wedges[72], and explore innovative applications of relict ground ice proxies to enable a more holistic perspective on paleoenvironmental change.

In summary, recent studies of wedge- and pore-ice stable isotope records have contributed substantially to knowledge of Quaternary climate dynamics in the Arctic. Continued focus on the key research directions outlined above will help this emerging discipline to reach its full potential in the field of Arctic paleoclimate studies.

Acknowledgements.

The authors thank Christopher Burn and two anonymous reviewers for their comments that improved this paper. T.J. Porter acknowledges the Natural Sciences and Engineering Research Council of Canada (Discovery Grant) for financial support.

Data availability. Coordinates of study sites, wedge-ice $\delta^{18}O$ data plotted in Figures 1 and 3 and relevant references are provided in Supplementary Table S1.

References

1. Schirrmeister L, Kunitsky V, Grosse G, et al. Sedimentary characteristics and origin of the Late Pleistocene Ice Complex on north-east Siberian Arctic coastal lowlands and islands – A review. *Quat Int*. 2011;241(1-2):3-25.
2. Murton JB, Goslar T, Edwards ME, et al. Palaeoenvironmental Interpretation of Yedoma Silt (Ice Complex) Deposition as Cold-Climate Loess, Duvanny Yar, Northeast Siberia. *Permafr Periglac Process*. 2015;26(3):208-288.
3. French H, Shur Y. The principles of cryostratigraphy. *Earth-Science Rev*. 2010;101:190-206.
4. Zazula GD, Froese DG, Schweger CE, et al. Palaeobotany: Ice-age steppe vegetation in east Beringia. *Nature*. 2003;423:603.
5. Sher AV, Kuzmina SA, Kuznetsova TV, Sulerzhitsky LD. New insights into the Weichselian environment and climate of the East Siberian Arctic, derived from fossil insects, plants, and mammals. *Quat Sci Rev*. 2005;24(5-6):533-569.
6. Kienast F, Wetterich S, Schirrmeister L, et al. Paleontological records indicate the occurrence of open woodlands in a dry inland climate at the present-day Arctic coast in western Beringia during the Last Interglacial. *Quat Sci Rev*. 2011;30(17-18):2134-2159.
7. Andreev AA, Schirrmeister L, Tarasov PE, et al. Vegetation and climate history in the Laptev Sea region (Arctic Siberia) during Late Quaternary inferred from pollen records. *Quat Sci Rev*. 2011;30(17-18):2182-2199.

8. Meyer H, Opel T, Laepple T, Dereviagin AY, Hoffmann K, Werner M. Long-term winter warming trend in the Siberian Arctic during the mid- to late Holocene. *Nat Geosci*. 2015;8:122-125.

9. Opel T, Wetterich S, Meyer H, Dereviagin AY, Fuchs MC, Schirrmeister L. Ground-ice stable isotopes and cryostratigraphy reflect late Quaternary palaeoclimate in the Northeast Siberian Arctic (Oyogos Yar coast, Dmitry Laptev Strait). *Clim Past*. 2017;13:587-611.

10. Dansgaard W. Stable isotopes in precipitation. *Tellus*. 1964;16:436-468.

11. Opel T, Meyer H, Wetterich S, Laepple T, Dereviagin A, Murton J. Ice wedges as archives of winter paleoclimate: A review. *Permafr Periglac Process*. 2018;29(3):199-209.

12. Schwamborn G, Meyer H, Fedorov G, Schirrmeister L, Hubberten H-W. Ground ice and slope sediments archiving late Quaternary paleoenvironment and paleoclimate signals at the margins of El'gygytgyn Impact Crater, NE Siberia. *Quat Res*. 2006;66:259-272.

13. Porter TJ, Schoenemann SW, Davies LJ, Steig EJ, Bandara S, Froese DG. Recent summer warming in northwestern Canada exceeds the Holocene thermal maximum. *Nat Commun*. 2019;10(1):1631 (1-10).

14. Dansgaard W, Johnsen SJ, Møller J, Langway CC. One thousand centuries of climatic record from Camp Century on the Greenland ice sheet. *Science*. 1969;166(3903):377-380.

15. Vasil'chuk YK. *[In Russian] Oxygen Isotope Composition of Ground Ice (Application to Paleogeocryological Reconstructions). Vol 1*. Moscow: Geological Faculty of Moscow State University; 1992.

16. Kotler E, Burn CR. Cryostratigraphy of the Klondike "muck" deposits, west-central Yukon Territory. *Can J Earth Sci*. 2000;37:849-861.

17. Stenni B, Masson-Delmotte V, Selmo E, et al. The deuterium excess records of EPICA Dome C and Dronning Maud Land ice cores (East Antarctica). *Quat Sci Rev*.

2010;29(1-2):146-159.

18. Meyer H, Schirrmeister L, Yoshikawa K, et al. Permafrost evidence for severe winter cooling during the Younger Dryas in northern Alaska. *Geophys Res Lett*. 2010;37.

19. Bartlein PJ, Harrison SP, Brewer S, et al. Pollen-based continental climate reconstructions at 6 and 21 ka: a global synthesis. *Clim Dyn*. 2011;37:775-802.

20. PAGES2k Consortium. A global multiproxy database for temperature reconstructions of the Common Era. *Sci Data*. 2017;4(170088).

21. Konecky B, McKay N, Churakova (Sidorova) O, et al. The Iso2k Database: A global compilation of paleo-δ18O and δ2H records to aid understanding of Common Era climate. *Earth Syst Sci Data Discuss*. 2020:1-49.

22. Lacelle D, Vasil'chuck Y. Recent progress (2007–2012) in permafrost isotope geochemistry. *Permafr Periglac Process*. 2013;24:138-145.

23. Streletskaya ID, Vasiliev AA, Oblogov GE, Tokarev IV. Reconstruction of paleoclimate of Russian Arctic in the Late Pleistocene-Holocene on the basis of isotope study of ice wedges. *Kriosf Zemli*. 2015;19:86-94.

24. Obu J, Westermann S, Bartsch A, et al. Northern Hemisphere permafrost map based on TTOP modelling for 2000–2016 at 1 km2 scale. *Earth-Science Rev*. 2019;193:299-316.

25. Leffingwell E deK. Ground-ice wedges, the dominant form of ground ice on the north coast of Alaska. *J Geol*. 1915;23:635-654.

26. Michel FA. *Isotope Investigations of Permafrost Waters in Northern Canada (PhD Thesis)*. University of Waterloo; 1982.

27. St-Jean M, Lauriol B, Clark ID, Lacelle D, Zdanowicz C. Investigation of ice-wedge infilling processes using stable oxygen and hydrogen isotopes, crystallography and occluded gases (O2, N2, Ar). *Permafr Periglac Process*. 2011;22(1):49-64.

28. Boereboom T, Samyn D, Meyer H, Tison J. Stable isotope and gas properties of two climatically contrasting (Pleistocene and Holocene) ice wedges from Cape Mamontov Klyk, Laptev Sea, northern Siberia. *Cryosph*. 2013;7:31-46.

29. Kim K, Yang J-W, Yoon H, et al. Greenhouse gas formation in ice wedges at Cyuie, central Yakutia. *Permafr Periglac Process*. 2019;30(1):48-57.

30. Porter TJ, Froese DG, Feakins SJ, et al. Multiple water isotope proxy reconstruction of extremely low last glacial temperatures in Eastern Beringia (Western Arctic). *Quat Sci Rev*. 2016;137:113-125.

31. Lacelle D. On the δ18O, δD and d-excess relations in meteoric precipitation and during equilibrium freezing: theoretical approach and field examples. *Permafr Periglac Process*. 2011;22:13-25.

32. Lacelle D, Fontaine M, Forest AP, Kokelj S. High-resolution stable water isotopes as tracers of thaw unconformities in permafrost: A case study from western Arctic Canada. *Chem Geol*. 2014;368:85-96.

33. Jouzel J. Calibrating the isotopic paleothermometer. *Science*. 1999;286:910-911.

34. Werner M, Haese B, Xu X, Zhang X, Butzin M, Lohmann G. H218O, HDO and deuterium excess – results from the fully coupled ECHAM5/MPI-OM Earth system model. *Geosci Model Dev*. 2016;9(2):647-670.

35. Schrag DP, Adkins JF, McIntyre K, et al. The oxygen isotopic composition of seawater during the Last Glacial Maximum. *Quat Sci Rev*. 2002;21:331-342.

36. Sundqvist HS, Kaufman DS, McKay NP, et al. Arctic Holocene proxy climate database - new approaches to assessing geochronological accuracy and encoding climate variables. *Clim Past*. 2014;10(4):1605-1631.

37. Meyer H, Schirrmeister L, Andreev A, et al. Lateglacial and Holocene isotopic and environmental history of northern coastal Alaska – Results from a buried ice-wedge system at Barrow. *Quat Sci Rev*. 2010;29(27-28):3720-3735.

38. Lachniet MS, Lawson DE, Sloat AR. Revised 14C dating of ice wedge growth in interior Alaska (USA) to MIS 2 reveals cold paleoclimate and carbon recycling in ancient permafrost terrain. *Quat Res*. 2012;78(2):217-225.

39. Schirrmeister L, Andreev A, Wetterich S, et al. Late Quaternary paleoenvironmental records from the Chatanika River valley near Fairbanks (Alaska). *Quat Sci Rev*.

2016;147:259-278.

40. Wetterich S, Rudaya N, Tumskoy V, et al. Last Glacial Maximum records in permafrost of the East Siberian Arctic. *Quat Sci Rev*. 2011;30:3139-3151.

41. Wetterich S, Tumskoy V, Rudaya N, et al. Ice Complex formation in arctic East Siberia during the MIS3 Interstadial. *Quat Sci Rev*. 2014;84:39-55.

42. Wetterich S, Tumskoy V, Rudaya N, et al. Ice Complex permafrost of MIS5 age in the Dmitry Laptev Strait coastal region (East Siberian Arctic). *Quat Sci Rev*. 2016;147:298-311.

43. Wetterich S, Rudaya N, Kuznetsov V, et al. Ice Complex formation on Bol'shoy Lyakhovsky Island (New Siberian Archipelago, East Siberian Arctic) since about 200 ka. *Quat Res*. 2019;92:530-548.

44. Froese DG, Westgate JA, Reyes A V, Enkin RJ, Preece SJ. Ancient permafrost and a future, warmer Arctic. *Science*. 2008;321:1648.

45. Andreev AA, Grosse G, Schirrmeister L, et al. Late Saalian and Eemian palaeoenvironmental history of the Bol'shoy Lyakhovsky Island (Laptev Sea region, Arctic Siberia). *Boreas*. 2004;33(4):319-348.

46. Vasil'chuk YK, van der Plicht J, Jungner H, Sonninen E, Vasil'chuk AC. First direct dating of Late Pleistocene ice-wedges by AMS. *Earth Planet Sci Lett*. 2000;179(2):237-242.

47. Grinter M, Lacelle D, Baranova N, Murseli S, Clark ID. Late Pleistocene and Holocene ice-wedge activity on the Blackstone Plateau, central Yukon, Canada. *Quat Res*. 2019;91(1):179-193.

48. Blinov A, Alfimov V, Beer J, et al. Ratio of 36 Cl/Cl in ground ice of east Siberia and its application for chronometry. *Geochemistry, Geophys Geosystems*. 2009;10(11):1-12.

49. NEEM Community Members. Eemian interglacial reconstructed from a Greenland folded ice core. *Nature*. 2013;493:489-494.

50. Opel T, Laepple T, Meyer H, Dereviagin AY, Wetterich S. Northeast Siberian ice wedges confirm Arctic winter warming over the past two millennia. *The Holocene*.

2017;27(11):1789-1796.

51. Froese DG, Zazula GD, Reyes A V. Seasonality of the late Pleistocene Dawson tephra and exceptional preservation of a buried riparian surface in central Yukon Territory, Canada. *Quat Sci Rev*. 2006;25:1542-1551.

52. Opel T, Murton JB, Wetterich S, et al. Middle and Late Pleistocene climate and continentality inferred from ice wedges at Batagay megaslump in the Northern Hemisphere's most continental region, Yana Highlands, interior Yakutia. *Clim Past*. 2019;15:1443-1461.

53. Vasil'chuk Y, Vasil'chuk A. Spatial distribution of mean winter air temperatures in Siberian permafrost at 20−18 ka BP using oxygen isotope data. *Boreas*. 2014;43(3):678-687.

54. Bowen GJ, Wassenaar LI, K.A. H. Global application of stable hydrogen and oxygen isotopes to wildlife forensics. *Oecologia*. 2005;143:337-348.

55. Vasil'chuk YK, Budantseva NA, Farquharson LM, Maslakov AA, Vasil'chuk AC, Chizhova JN. Isotopic evidence for Holocene January air temperature variability on the East Chukotka Peninsula. *Permafr Periglac Process*. 2018;29(4):283-297.

56. Streletskaya I, Vasiliev A, Meyer H. Isotopic composition of syngenetic ice wedges and palaeoclimatic reconstruction, western Taymyr, Russian Arctic. *Permafr Periglac Process*. 2011;22(1):101-106.

57. Vasil'chuk YK, Budantseva NA, Christiansen HH, Chizhova JN, Vasil'chuk AC, Zemskova AM. Oxygen stable isotope variation in Late Holocene ice wedges in Yamal Peninsula and Svalbard. *Geogr Environ Sustain*. 2015;8:36-54.

58. Laskar J, Fienga A, Gastineau M, Manche H. La2010: a new orbital solution for the long-term motion of the Earth. *Astron Astrophys*. 2011;532:A89.

59. Marcott SA, Shakun JD, Clark PU, Mix AC. A reconstruction of regional and global temperature for the past 11,300 years. *Science*. 2013;339:1198-1201.

60. Vasil'chuk YK. Syngenetic Ice Wedges: Cyclical Formation, Radiocarbon Age and Stable Isotope Records by Yurij K. Vasil ' chuk, Moscow University Press, Moscow,

2006. 404 pp. ISBN 5-211-05212 - 9. *Permafr Periglac Process*. 2013;24(1):82-93.

61. Johnsen SJ, Dahl-Jensen D, Gundestrup N, et al. Oxygen isotope and palaeotemperature records from six Greenland ice-core stations: Camp Century, Dye-3, GRIP, GISP2, Renland and NorthGRIP. *J Quat Sci*. 2001;16:299-307.

62. Vasil'chuk YK, Vasil'chuk AC. Winter air paleotemperatures at 30-12 kyr BP in the Lower Kolyma River, Plankhinskii Yar Yedoma: Evidence from stable isotopes. *Earth's Cryosph*. 2018;22:3-16.

63. Vasil'chuk YK, Budantseva NA, Bartova AV, Zimov SA. Variations of stable oxygen isotopes in ice wedges of the cyclite yedoma of Stanchikovsky Yar on the Maly Anyuy River. *Arct Antarct*. 2018:37-56.

64. Vasil'chuk YK, Vasil'chuk AC. The Oxygen Isotope Composition of Ice Wedges of Ayon Island and Paleotemperature Reconstructions of the Late Pleistocene and Holocene of the Northern Chukotka. *Moscow Univ Geol Bull*. 2018;73:87-99.

65. Vasil'chuk YK, Vasil'chuk AC. Ice wedges in the Mayn River Valley and winter air paleotemperatures in the Souther Chukchi Peninsula at 38-12 kyr BP. *Earth's Cryosph*. 2017;21:24-35.

66. Vasil'chuk YK, Vasil'chuk JY, Budantseva NA, Vasil'chuk AC. Isotopic and geochemical features of the Batagaika yedoma (preliminary results). *Arct Antarct*. 2017:69-96.

67. Mackay JR. Offshore permafrost and ground ice, southern Beaufort Sea. *Can J Earth Sci*. 1972;9:1550-1561.

68. Michel FA, Fritz P. Significance of isotope variations in permafrost waters at Illisarvik, N.W.T. *Proc 4th Can Permafr Conf*. 1982:173-181.

69. Fritz M, Wetterich S, Schirrmeister L, et al. Eastern Beringia and beyond: Late Wisconsinan and Holocene landscape dynamics along the Yukon Coastal Plain, Canada. *Palaeogeogr Palaeoclimatol Palaeoecol*. 2012;319-320:28-45.

70. Michel FA. Isotopic composition of ice-wedge ice in northwestern Canada. *Proc 5th Can Permafr Conf*. 1990:5-9.

71. Steffensen JP, Andersen KK, Bigler M, et al. High-resolution Greenland ice core data show abrupt climate change happens in few years. *Science*. 2008;321:680-684.

72. Iizuka Y, Miyamoto C, Matoba S, et al. Ion concentrations in ice wedges: An innovative approach to reconstruct past climate variability. *Earth Planet Sci Lett*. 2019;515:58-66.

73. Praetorius SK, Mix AC. Synchronization of North Pacific and Greenland climates preceded abrupt deglacial warming. *Science*. 2014;345:444-448.

74. Lachniet MS, Lawson DE, Stephen H, Sloat AR, Patterson WP. Isoscapes of δ18O and δ2H reveal climatic forcings on Alaska and Yukon precipitation. *Water Resour Res*. 2016;52:6575–6586.

75. Meyer H, Yoshikawa K, Schirrmeister L, Andreev A. The Vault Creek Tunnel (Fairbanks region, Alaska); a late Quaternary palaeoenvironmental permafrost record. *9th Int Conf Permafr Proc*. 2008:1191-1196.

76. Lacelle D, St-Jean M, Lauriol B, et al. Burial and preservation of a 30,000 year old perennial snowbank in Red Creek valley, Ogilvie Mountains, central Yukon, Canada. *Quat Sci Rev*. 2009;28(27-28):3401-3413.

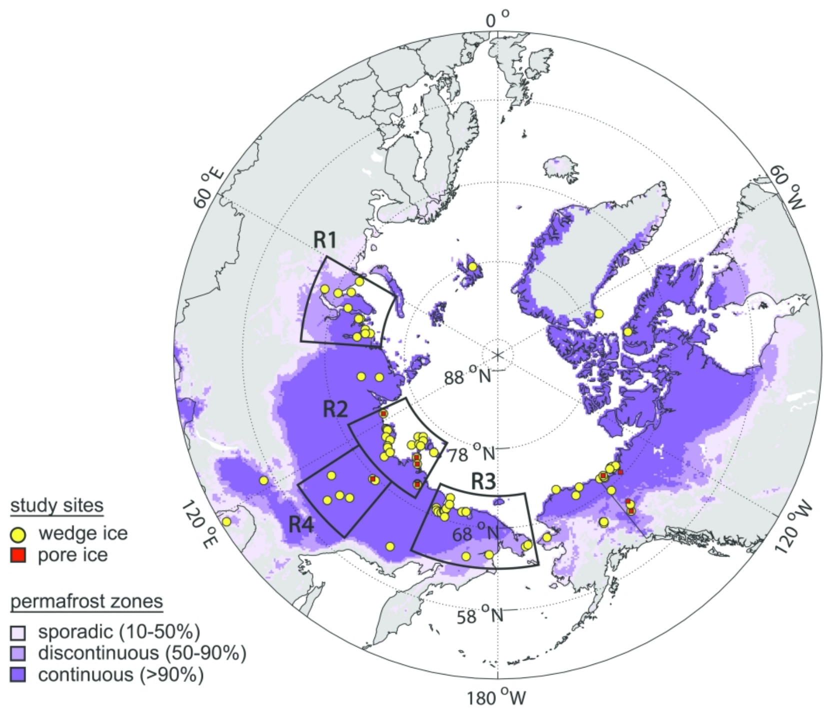

Figure 1. Sites of recent studies of water isotopes in relict wedge ice (yellow circles) and pore ice (red squares); Russian sub-regions of W. Siberia (R1), Laptev Sea region (R2), Kolyma and Chukotka (R3) and central Yakutia (R4) are indicated; modelled permafrost zones[24] are indicated.

320x254mm (300 x 300 DPI)

Figure 2. Ice-wedge and pore-ice sampling. (A) Ice-wedge sampling by chainsaw; (B,C) block cuts from an ice wedge; (D) slice cut from an ice wedge; (E) internal foliation of an ice wedge with visible ice veins and sediment and organic inclusions; (F) pore-ice sampling by lateral coring of a permafrost exposure using a hand-held drill; (G) pore-ice sampling by vertical coring into permafrost using a gas-powered drill; and (H) recovering the permafrost core from the 'core catcher'.

544x449mm (300 x 300 DPI)

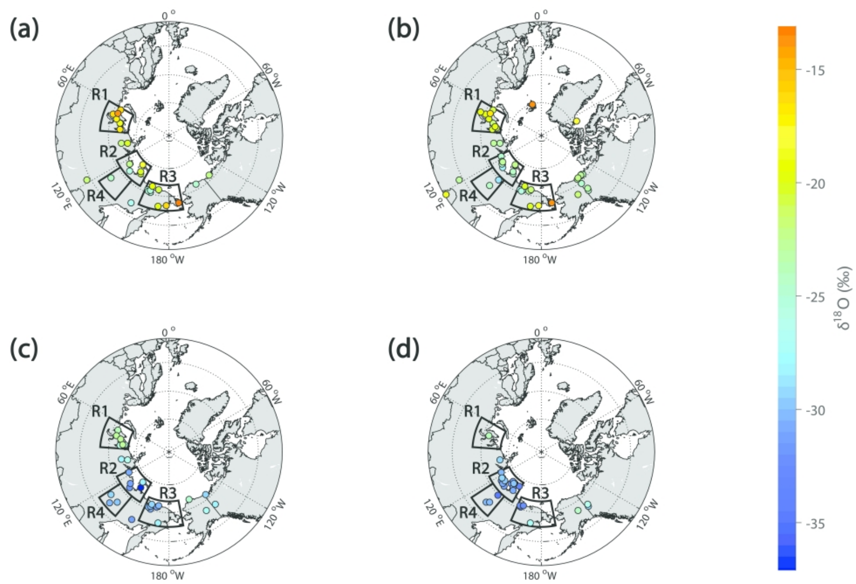

Figure 3. Average wedge-ice δ^{18}O values dating to (a) modern, (b) Holocene, (c) MIS 2 and (d) MIS 3 from studies since 2010 (see Table S1 for data and sources); Russian sub-regions of W. Siberia (R1), Laptev Sea region (R2), Kolyma and Chukotka (R3) and central Yakutia (R4) are indicated.

382x254mm (500 x 500 DPI)

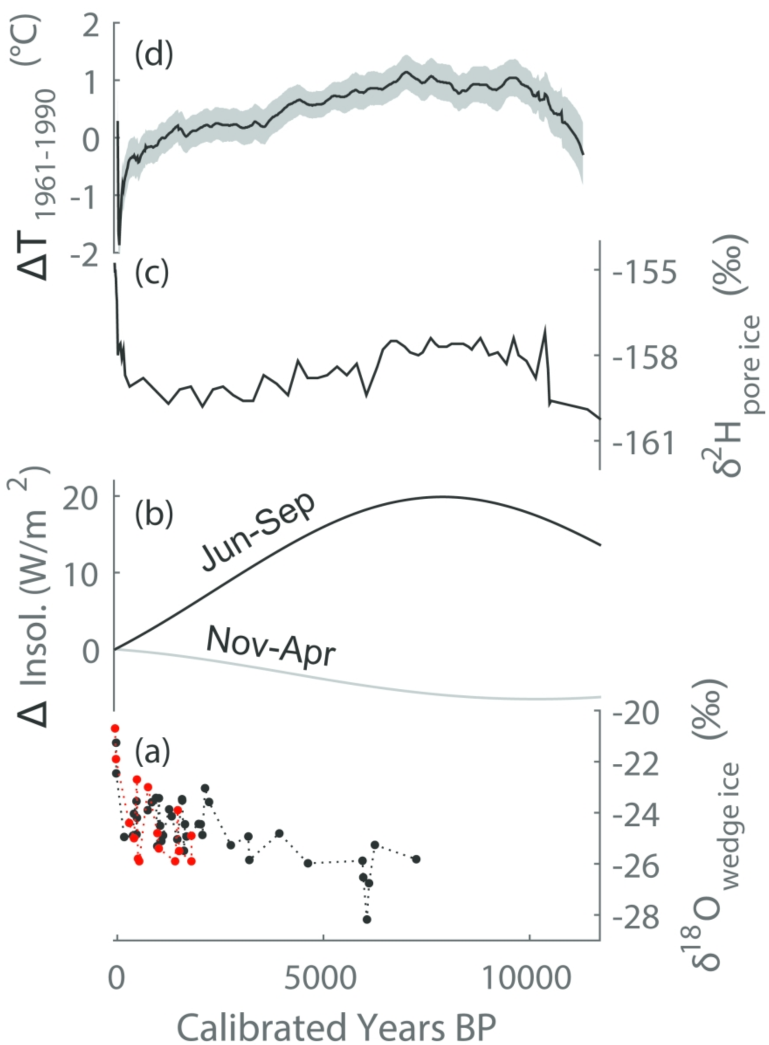

Figure 4. Holocene paleoclimate reconstructions and relict ground-ice water-isotope records. (a) Multi-site stacked wedge-ice $\delta^{18}O$ record from the Lena Delta[8] (black dashed line) and a single-site stacked wedge-ice $\delta^{18}O$ record from the Oyogos Yar coast[50] (red dashed line); (b) insolation change relative to modern during the warm-season (Jun-Sep) and cold-season (Nov-Apr) after Laskar et al.[58]; (c) pore-ice $\delta^{2}H$ record from DHP174 site in central Yukon[13]; (d) Northern Hemisphere multi-proxy temperature reconstruction[59].

123x167mm (500 x 500 DPI)

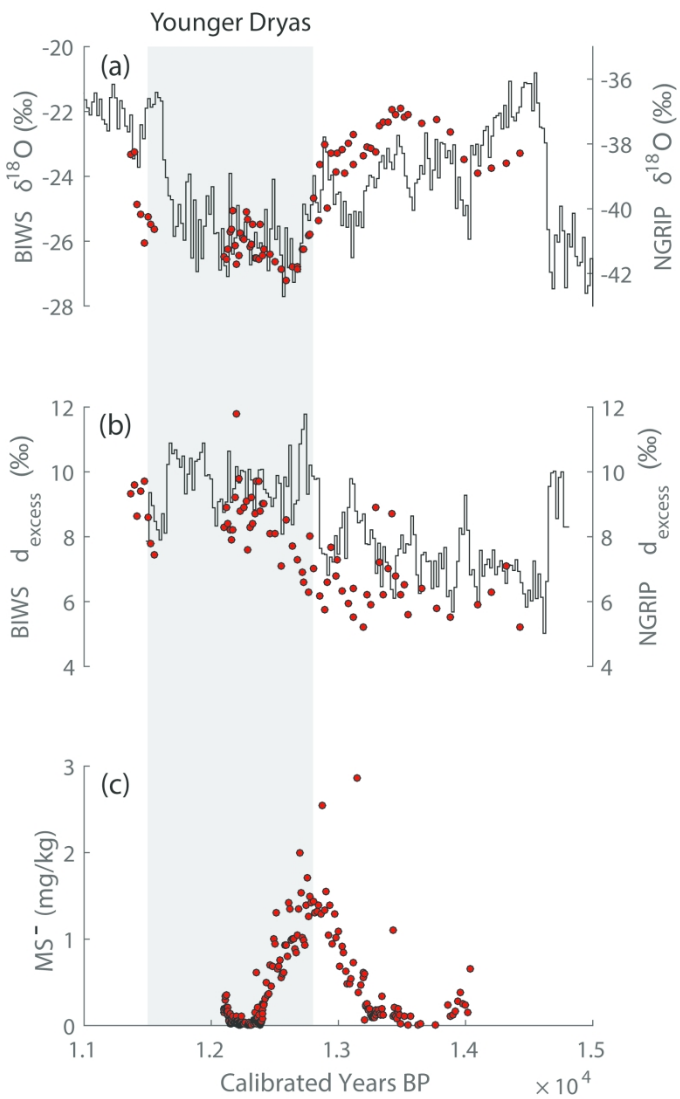

Figure 5. Water isotope and phytoplankton-derived methanesulfonate ion (MS^-) records dating to the Younger Dryas transition from the Barrow Ice Wedge System (BIWS) and NGRIP ice core. (a, b) $\delta^{18}O$ and d_{excess} records from BIWS[18] (red circles) and NGRIP[71] (black line). (c) MS- ion concentration from BIWS[72] (red circles).

165x254mm (300 x 300 DPI)

Site ID	Country	Site name	Latitude	Longitude
1	Russia	Amderma	70.00	62.00
2	Russia	Marre-Sale Cape	69.68	66.80
3	Russia	Erkutayakha River	68.19	68.86
4	Russia	Shchuchya River	66.50	69.00
5	Russia	Seyakha Vostochnaya River	70.00	72.50
6	Russia	Gydan Peninsula	71.80	75.20
7	Russia	Era-Maretayakha	71.65	75.42
8	Russia	Sibiryakov Island	72.72	79.10
9	Russia	Dikson	73.52	80.57
10	Russia	Krestyanka River	72.90	80.90
11	Russia	Sopochnaya Karga Cape	71.90	82.60
12	Russia	Labaz Lake	72.33	99.00
13	Russia	Cape Sabler	74.55	100.53
14	Russia	Mamontov Klyk	73.60	117.17
15	Russia	Chara River	56.77	118.10
16	Russia	Nagym, Lena Delta	72.90	123.20
17	Russia	Turakh, Lena Delta	72.97	123.80
18	Russia	Khardang, Lena Delta	73.00	124.20
19	Russia	Vilyui near Tyalychima River	64.00	126.00
20	Russia	Central Lena Delta	72.38	126.12
21	Russia	Kurungnakh, Lena Delta	72.30	126.30
22	Russia	Sobo Sise, Lena Delta	72.50	128.30
23	Russia	Bykovsky Peninsula	71.78	129.43
24	Russia	Muostakh Island	71.60	130.00
25	Russia	Cyuie	61.73	130.42
26	Russia	Tanda	63.30	131.70
27	Russia	Kular	70.63	131.88
28	Russia	Buor Khaya	71.50	132.10
29	Russia	Mamontova Gora	64.00	134.00
30	Russia	Batagay	67.60	134.80
31	Russia	Adycha	67.66	135.69
32	Russia	Belkovsky Island	75.40	135.60
33	Russia	Stolbovoy Island	74.10	136.10
34	Russia	Kotelny Island, north coast	75.80	137.50
35	Russia	Kotelny Island	74.70	138.50
36	Russia	Kotelny Island, Balyktakh river	75.43	138.82
37	Russia	Kotelny Island, south coast	74.80	139.60
38	Russia	Bol'shoy Lyakhovsky	73.30	141.50
39	Russia	Oyogos Yar	72.70	143.50
40	Russia	Novaya Sibir' Island	75.10	146.70
41	Russia	Boydom	70.64	148.15
42	Russia	Kryvaya	70.56	148.26
43	Russia	Pit Phoenix	62.25	150.75
44	Russia	Bison, Kolyma River basin	69.00	158.00
45	Russia	Alyoshkinskaya terrace	68.72	158.40
46	Russia	Duvanny Yar	68.63	159.15
47	Russia	Plakhinskii Yar	68.68	160.29
48	Russia	Zelyony Mys	69.00	161.00
49	Russia	Pokhodsk	69.04	161.01
50	Russia	Stanchikovsky Yar	69.37	161.52

51	Russia	Chetyrekhstolbovy Island	70.78	161.60
52	Russia	Krasivoe	68.30	161.73
53	Russia	Ambarchik Polar Station	70.00	162.00
54	Russia	Rauchua River	69.50	167.00
55	Russia	Ayon Island	69.63	168.58
56	Russia	Mayn River Valley	64.17	171.04
57	Russia	Anadyr Town	64.73	177.52
58	Russia	Lorino Settlement	65.50	-171.72
59	Russia	Lavrentiya Settlement	65.58	-170.99
60	Norway	Adventdalen	78.20	15.83
61	Denmark	Annikitisoq	76.03	-67.62
62	China	Yitulihe	50.62	121.53
63	USA	Northern Seward Peninsula	66.00	-165.00
64	USA	Barrow	71.30	-156.67
65	USA	Itkilik	69.57	-150.87
66	USA	Prudhoe Bay	70.20	-148.40
67	USA	Vault Creek Tunnel, Chatanika River	65.03	-147.70
68	USA	Fairbanks	64.80	-147.70
69	USA	CRREL Fox Tunnel	64.95	-147.62
70	Canada	Komakuk Beach	69.60	-140.50
71	Canada	Old Crow	67.58	-140.00
72	Canada	Klondike	64.06	-139.41
73	Canada	Kay Point	69.25	-139.19
74	Canada	Roland Bay	69.43	-139.00
75	Canada	Herschel Island	69.60	-138.96
76	Canada	Moose Lake	64.74	-138.37
77	Canada	DHP174	65.21	-138.32
78	Canada	Illisarvik	69.48	-134.59
79	Canada	Inuvik	68.39	-133.76
80	Canada	Hooper Island	69.69	-134.85
81	Canada	Richards Island, North Point	69.70	-134.24
82	Canada	Pingo Canadian Landmark area	69.41	-133.12
83	Canada	Pelly Island	69.63	-135.43
84	Canada	Bylot Island	73.16	-79.94

		ca. modern			Holocene	
Wedge ice	**Pore ice**	**δ18O**	**s.d.**	**n**	**δ18O**	**s.d.**
x	n/a	-16.5	n/a	4	-20.9	n/a
x	n/a	-14	n/a	2	-16.7	n/a
x	n/a	n/a	n/a	n/a	-19.6	0.7
x	n/a	n/a	n/a	n/a	-19.4	n/a
x	n/a	-17.3	n/a	2	-19.7	n/a
x	n/a	-18.8	n/a	3	-21.9	n/a
x	n/a	-19	n/a	n/a	n/a	n/a
x	n/a	n/a	n/a	n/a	-19.9	n/a
x	n/a	n/a	n/a	n/a	-20.7	n/a
x	n/a	n/a	n/a	n/a	n/a	n/a
x	n/a	-16.6	n/a	4	-20.3	n/a
x	n/a	-22	n/a	n/a	-23	n/a
x	n/a	-20.4	n/a	5	-23.1	n/a
x	x	-20.5	1	5	-24.6	n/a
x	n/a	-21.6	1.2	2	-22.6	2.2
x	n/a	n/a	n/a	n/a	-22.7	n/a
x	n/a	n/a	n/a	n/a	-22.9	n/a
x	n/a	n/a	n/a	n/a	n/a	n/a
x	n/a	-24.2	n/a	n/a	n/a	n/a
x	n/a	-22.2	n/a	12	-24.6	1.2
x	n/a	n/a	n/a	n/a	n/a	n/a
x	n/a	n/a	n/a	n/a	n/a	n/a
x	n/a	n/a	n/a	n/a	-28.2	n/a
x	n/a	n/a	n/a	n/a	n/a	n/a
x	n/a	n/a	n/a	n/a	n/a	n/a
x	n/a	n/a	n/a	n/a	n/a	n/a
x	n/a	-26	n/a	n/a	n/a	n/a
x	n/a	n/a	n/a	n/a	n/a	n/a
x	n/a	n/a	n/a	n/a	-24.2	n/a
x	x	n/a	n/a	n/a	n/a	n/a
x	n/a	n/a	n/a	n/a	-29	0.7
x	n/a	n/a	n/a	n/a	n/a	n/a
x	n/a	n/a	n/a	n/a	n/a	n/a
x	n/a	n/a	n/a	n/a	-22.5	0.4
x	n/a	-18	n/a	n/a	n/a	n/a
x	n/a	n/a	n/a	n/a	-25	1.2
x	n/a	n/a	n/a	n/a	n/a	n/a
x	x	-20.4	1.27	8	-24.2	1.1
x	x	-20.7	1.61	11	-25.1	1.1
x	n/a	n/a	n/a	n/a	n/a	n/a
x	x	n/a	n/a	n/a	-28.3	1
x	x	n/a	n/a	n/a	-26.1	0.4
x	n/a	-27	n/a	n/a	n/a	n/a
x	n/a	-25.3	n/a	7	-27	n/a
x	n/a	-26	n/a	n/a	n/a	n/a
x	n/a	-25.1	n/a	n/a	n/a	n/a
x	n/a	-25.8	n/a	n/a	-25.8	1.4
x	n/a	-25.5	n/a	n/a	n/a	n/a
x	n/a	n/a	n/a	n/a	-26.6	0.6
x	n/a	n/a	n/a	n/a	n/a	n/a

x	n/a	-19.2	n/a	14	-20.3	n/a
x	n/a	-26	n/a	n/a	n/a	n/a
x	n/a	n/a	n/a	n/a	n/a	n/a
x	n/a	n/a	n/a	n/a	-23	n/a
x	n/a	-20	n/a	n/a	-21.6	0.5
x	n/a	-20	n/a	n/a	-20.2	0.2
x	n/a	-16.1	n/a	2	-18.45	n/a
x	n/a	-13.1	n/a	4	-16.5	n/a
x	n/a	n/a	n/a	n/a	-14	n/a
x	n/a	n/a	n/a	n/a	-13.9	0.7
x	n/a	n/a	n/a	n/a	-18	0.8
x	n/a	n/a	n/a	n/a	-18.8	n/a
x	n/a	n/a	n/a	n/a	-17.3	n/a
x	n/a	n/a	n/a	n/a	-21.5	1.4
x	n/a	-25	n/a	3	n/a	n/a
x	n/a	n/a	n/a	n/a	-23.67	1.5
x	n/a	n/a	n/a	n/a	-21.9	n/a
x	n/a	n/a	n/a	n/a	n/a	n/a
x	n/a	n/a	n/a	n/a	n/a	n/a
x	n/a	n/a	n/a	n/a	-23.3	n/a
x	n/a	n/a	n/a	n/a	-25	1
x	x	n/a	n/a	n/a	-24.5	0.5
x	n/a	n/a	n/a	n/a	-19.14	0.6
x	n/a	n/a	n/a	n/a	-22.77	1.1
x	x	n/a	n/a	n/a	-22.1	n/a
x	n/a	n/a	n/a	n/a	-23.9	0.5
n/a	x	n/a	n/a	n/a	n/a	n/a
x	n/a	-22.5	n/a	1	n/a	n/a
n/a	x	n/a	n/a	n/a	n/a	n/a
x	n/a	n/a	n/a	n/a	-23	0.7
x	n/a	n/a	n/a	n/a	-24.6	0.8
x	n/a	n/a	n/a	n/a	-24	0.6
x	n/a	n/a	n/a	n/a	-25.2	0.4
x	n/a	n/a	n/a	n/a	-25.63	0.95

				Wedge-ice mean δ18O values organise			
	MIS2			MIS3			
n	δ18O	s.d.	n	δ18O	s.d.	n	δ18O
4	n/a	n/a	n/a	n/a	n/a	n/a	n/a
40	-23.9	n/a	126	n/a	n/a	n/a	n/a
18	n/a	n/a	n/a	n/a	n/a	n/a	n/a
7	n/a	n/a	n/a	n/a	n/a	n/a	n/a
3	-22.9	n/a	15	-23.9	n/a	17	n/a
40	-24.1	n/a	5	n/a	n/a	n/a	n/a
n/a	-23	n/a	n/a	n/a	n/a	n/a	n/a
22	n/a	n/a	n/a	n/a	n/a	n/a	n/a
17	-26	n/a	10	n/a	n/a	n/a	n/a
n/a	-22.6	n/a	17	n/a	n/a	n/a	n/a
9	-26	n/a	17	n/a	n/a	n/a	n/a
138	-28.32	n/a	9	n/a	n/a	n/a	n/a
8	-26.3	n/a	26	-29.5	n/a	24	n/a
122	-31.04	n/a	33	-30.5	0.7	4	n/a
48	n/a	n/a	n/a	n/a	n/a	n/a	n/a
5	n/a	n/a	n/a	-29.3	0.3	12	n/a
14	n/a	n/a	n/a	n/a	n/a	n/a	n/a
n/a	n/a	n/a	n/a	-30.1	1.3	10	n/a
n/a	-29.5	n/a	n/a	n/a	n/a	n/a	n/a
40	n/a	n/a	n/a	n/a	n/a	n/a	n/a
n/a	n/a	n/a	n/a	-31.6	0.6	11	n/a
n/a	n/a	n/a	n/a	-29.7	1.1	16	n/a
239	-31.17	n/a	36	-30.8	1.6	145	n/a
n/a	n/a	n/a	n/a	-31.9	1.2	85	n/a
n/a	-30.5	n/a	22	n/a	n/a	n/a	n/a
n/a	n/a	n/a	n/a	-30.5	0.3	10	n/a
n/a	-31.7	n/a	n/a	n/a	n/a	n/a	n/a
n/a	n/a	n/a	n/a	-31.2	1	26	n/a
4	-29.7	n/a	n/a	-30.5	0.6	18	n/a
n/a	n/a	n/a	n/a	-34.9	0.9	12	n/a
10	n/a	n/a	n/a	n/a	n/a	n/a	n/a
n/a	n/a	n/a	n/a	-31.3	0.4	21	n/a
n/a	n/a	n/a	n/a	-31.7	0.4	16	n/a
19	n/a	n/a	n/a	n/a	n/a	n/a	n/a
n/a	n/a	n/a	n/a	-29.8	1	17	n/a
15	-28.5	1.2	5	n/a	n/a	n/a	n/a
n/a	n/a	n/a	n/a	-30.3	0.2	8	n/a
90	-37.1	0.7	14	-31	1.2	196	-35.7
518	n/a	n/a	n/a	-30.8	1.3	150	n/a
n/a	n/a	n/a	n/a	-33.5	0.6	5	n/a
13	n/a	n/a	n/a	n/a	n/a	n/a	n/a
8	n/a	n/a	n/a	n/a	n/a	n/a	n/a
n/a	-31.5	n/a	n/a	n/a	n/a	n/a	n/a
6	n/a	n/a	n/a	-32.4	n/a	61	n/a
n/a	-31	n/a	n/a	n/a	n/a	n/a	n/a
n/a	-30.5	n/a	n/a	-32.6	1	9	n/a
5	-32.5	1.2	19	n/a	n/a	n/a	n/a
n/a	-30.5	n/a	n/a	n/a	n/a	n/a	n/a
7	n/a	n/a	n/a	n/a	n/a	n/a	n/a
n/a	-32.6	0.4	40	-32.1	0.6	30	n/a

3	n/a	n/a	n/a	n/a	n/a	n/a	n/a
n/a	-31	n/a	n/a	n/a	n/a	n/a	n/a
n/a	-29.2	n/a	5	n/a	n/a	n/a	n/a
3	-31.2	n/a	10	n/a	n/a	n/a	n/a
8	-30.4	1.1	60	n/a	n/a	n/a	n/a
2	-28	0.7	10	-27.2	0.8	12	n/a
21	n/a	n/a	n/a	n/a	n/a	n/a	n/a
62	n/a	n/a	n/a	n/a	n/a	n/a	n/a
30	n/a	n/a	n/a	n/a	n/a	n/a	n/a
65	n/a	n/a	n/a	n/a	n/a	n/a	n/a
30	n/a	n/a	n/a	n/a	n/a	n/a	n/a
16	n/a	n/a	n/a	n/a	n/a	n/a	n/a
n/a	-24.3	n/a	n/a	n/a	n/a	n/a	n/a
14	-24.4	1.8	121	n/a	n/a	n/a	n/a
n/a	n/a	n/a	n/a	n/a	n/a	n/a	n/a
22	n/a	n/a	n/a	n/a	n/a	n/a	n/a
n/a	n/a	n/a	n/a	n/a	n/a	n/a	n/a
n/a	-26.9	n/a	n/a	n/a	n/a	n/a	n/a
n/a	-27.2	n/a	n/a	n/a	n/a	n/a	n/a
25	n/a	n/a	n/a	n/a	n/a	n/a	n/a
46	n/a	n/a	n/a	n/a	n/a	n/a	n/a
3	n/a	n/a	n/a	-29.3	0.6	3	n/a
2	n/a	n/a	n/a	n/a	n/a	n/a	n/a
7	-26.8	1.1	2	n/a	n/a	n/a	n/a
105	-29.1	n/a	18	n/a	n/a	n/a	n/a
93	-28.5	1.2	107	-26.4	0.5	19	n/a
n/a	n/a	n/a	n/a	n/a	n/a	n/a	n/a
n/a	n/a	n/a	n/a	n/a	n/a	n/a	n/a
n/a	n/a	n/a	n/a	n/a	n/a	n/a	n/a
220	n/a	n/a	n/a	n/a	n/a	n/a	n/a
209	n/a	n/a	n/a	n/a	n/a	n/a	n/a
275	n/a	n/a	n/a	n/a	n/a	n/a	n/a
99	n/a	n/a	n/a	n/a	n/a	n/a	n/a
41	n/a	n/a	n/a	n/a	n/a	n/a	n/a

ed by time-slice

MIS4		MIS5			MIS6		
s.d.	n	δ18O	s.d.	n	δ18O	s.d.	n
n/a	n/a	n/a	n/a	n/a	n/a	n/a	n/a
n/a	n/a	n/a	n/a	n/a	n/a	n/a	n/a
n/a	n/a	n/a	n/a	n/a	n/a	n/a	n/a
n/a	n/a	n/a	n/a	n/a	n/a	n/a	n/a
n/a	n/a	n/a	n/a	n/a	n/a	n/a	n/a
n/a	n/a	n/a	n/a	n/a	n/a	n/a	n/a
n/a	n/a	n/a	n/a	n/a	n/a	n/a	n/a
n/a	n/a	n/a	n/a	n/a	n/a	n/a	n/a
n/a	n/a	n/a	n/a	n/a	n/a	n/a	n/a
n/a	n/a	n/a	n/a	n/a	n/a	n/a	n/a
n/a	n/a	n/a	n/a	n/a	n/a	n/a	n/a
n/a	n/a	n/a	n/a	n/a	n/a	n/a	n/a
n/a	n/a	n/a	n/a	n/a	n/a	n/a	n/a
n/a	n/a	n/a	n/a	n/a	n/a	n/a	n/a
n/a	n/a	n/a	n/a	n/a	n/a	n/a	n/a
n/a	n/a	n/a	n/a	n/a	n/a	n/a	n/a
n/a	n/a	n/a	n/a	n/a	n/a	n/a	n/a
n/a	n/a	n/a	n/a	n/a	n/a	n/a	n/a
n/a	n/a	n/a	n/a	n/a	n/a	n/a	n/a
n/a	n/a	n/a	n/a	n/a	n/a	n/a	n/a
n/a	n/a	n/a	n/a	n/a	n/a	n/a	n/a
n/a	n/a	n/a	n/a	n/a	n/a	n/a	n/a
n/a	n/a	n/a	n/a	n/a	n/a	n/a	n/a
n/a	n/a	n/a	n/a	n/a	n/a	n/a	n/a
n/a	n/a	n/a	n/a	n/a	n/a	n/a	n/a
n/a	n/a	n/a	n/a	n/a	n/a	n/a	n/a
n/a	n/a	n/a	n/a	n/a	n/a	n/a	n/a
n/a	n/a	n/a	n/a	n/a	n/a	n/a	n/a
n/a	n/a	n/a	n/a	n/a	n/a	n/a	n/a
n/a	n/a	n/a	n/a	n/a	n/a	n/a	n/a
n/a	n/a	n/a	n/a	n/a	n/a	n/a	n/a
n/a	n/a	n/a	n/a	n/a	n/a	n/a	n/a
n/a	n/a	n/a	n/a	n/a	n/a	n/a	n/a
n/a	n/a	n/a	n/a	n/a	n/a	n/a	n/a
n/a	n/a	n/a	n/a	n/a	n/a	n/a	n/a
n/a	n/a	n/a	n/a	n/a	n/a	n/a	n/a
n/a	n/a	n/a	n/a	n/a	n/a	n/a	n/a
0.7	37	-33	0.3	9	n/a	n/a	n/a
n/a	n/a	-33.1	0.3	7	n/a	n/a	n/a
n/a	n/a	n/a	n/a	n/a	n/a	n/a	n/a
n/a	n/a	n/a	n/a	n/a	n/a	n/a	n/a
n/a	n/a	n/a	n/a	n/a	n/a	n/a	n/a
n/a	n/a	n/a	n/a	n/a	n/a	n/a	n/a
n/a	n/a	n/a	n/a	n/a	n/a	n/a	n/a
n/a	n/a	n/a	n/a	n/a	n/a	n/a	n/a
n/a	n/a	n/a	n/a	n/a	n/a	n/a	n/a
n/a	n/a	n/a	n/a	n/a	n/a	n/a	n/a
n/a	n/a	n/a	n/a	n/a	n/a	n/a	n/a
n/a	n/a	n/a	n/a	n/a	n/a	n/a	n/a
n/a	n/a	n/a	n/a	n/a	n/a	n/a	n/a

n/a	n/a	n/a	n/a	n/a	n/a	n/a	n/a
n/a	n/a	n/a	n/a	n/a	n/a	n/a	n/a
n/a	n/a	n/a	n/a	n/a	n/a	n/a	n/a
n/a	n/a	n/a	n/a	n/a	n/a	n/a	n/a
n/a	n/a	n/a	n/a	n/a	n/a	n/a	n/a
n/a	n/a	n/a	n/a	n/a	n/a	n/a	n/a
n/a	n/a	n/a	n/a	n/a	n/a	n/a	n/a
n/a	n/a	n/a	n/a	n/a	n/a	n/a	n/a
n/a	n/a	n/a	n/a	n/a	n/a	n/a	n/a
n/a	n/a	n/a	n/a	n/a	n/a	n/a	n/a
n/a	n/a	n/a	n/a	n/a	n/a	n/a	n/a
n/a	n/a	n/a	n/a	n/a	n/a	n/a	n/a
n/a	n/a	n/a	n/a	n/a	n/a	n/a	n/a
n/a	n/a	n/a	n/a	n/a	n/a	n/a	n/a
n/a	n/a	n/a	n/a	n/a	n/a	n/a	n/a
n/a	n/a	n/a	n/a	n/a	n/a	n/a	n/a
n/a	n/a	n/a	n/a	n/a	n/a	n/a	n/a
n/a	n/a	n/a	n/a	n/a	n/a	n/a	n/a
n/a	n/a	n/a	n/a	n/a	n/a	n/a	n/a
n/a	n/a	n/a	n/a	n/a	n/a	n/a	n/a
n/a	n/a	n/a	n/a	n/a	n/a	n/a	n/a
n/a	n/a	n/a	n/a	n/a	n/a	n/a	n/a
n/a	n/a	n/a	n/a	n/a	n/a	n/a	n/a
n/a	n/a	n/a	n/a	n/a	n/a	n/a	n/a
n/a	n/a	n/a	n/a	n/a	n/a	n/a	n/a
n/a	n/a	n/a	n/a	n/a	n/a	n/a	n/a
n/a	n/a	n/a	n/a	n/a	n/a	n/a	n/a
n/a	n/a	n/a	n/a	n/a	n/a	n/a	n/a
n/a	n/a	n/a	n/a	n/a	n/a	n/a	n/a
n/a	n/a	n/a	n/a	n/a	n/a	n/a	n/a
n/a	n/a	n/a	n/a	n/a	n/a	n/a	n/a
n/a	n/a	n/a	n/a	n/a	n/a	n/a	n/a
n/a	n/a	n/a	n/a	n/a	n/a	n/a	n/a
n/a	n/a	n/a	n/a	n/a	n/a	n/a	n/a

MIS7 or older			
δ18O	s.d.	n	Stated in cited papers
n/a	n/a	n/a	x
n/a	n/a	n/a	x
n/a	n/a	n/a	n/a
n/a	n/a	n/a	x
n/a	n/a	n/a	x
n/a	n/a	n/a	x
n/a	n/a	n/a	x
n/a	n/a	n/a	x
n/a	n/a	n/a	x
n/a	n/a	n/a	x
n/a	n/a	n/a	x
n/a	n/a	n/a	x
n/a	n/a	n/a	x
n/a	n/a	n/a	x
n/a	n/a	n/a	n/a
n/a	n/a	n/a	x
n/a	n/a	n/a	x
n/a	n/a	n/a	x
n/a	n/a	n/a	x
n/a	n/a	n/a	x
n/a	n/a	n/a	x
n/a	n/a	n/a	x
n/a	n/a	n/a	x
n/a	n/a	n/a	x
n/a	n/a	n/a	x
n/a	n/a	n/a	x
n/a	n/a	n/a	x
n/a	n/a	n/a	x
n/a	n/a	n/a	x
-33.1	0.1	6	x
n/a	n/a	n/a	x
n/a	n/a	n/a	x
n/a	n/a	n/a	x
n/a	n/a	n/a	x
n/a	n/a	n/a	x
n/a	n/a	n/a	n/a
n/a	n/a	n/a	n/a
-31.8	1.25	56	x
n/a	n/a	n/a	x
n/a	n/a	n/a	x
n/a	n/a	n/a	x
n/a	n/a	n/a	x
n/a	n/a	n/a	x
n/a	n/a	n/a	x
n/a	n/a	n/a	x
n/a	n/a	n/a	x
n/a	n/a	n/a	n/a
n/a	n/a	n/a	x
n/a	n/a	n/a	x
n/a	n/a	n/a	n/a

n/a	n/a	n/a	x
n/a	n/a	n/a	x
n/a	n/a	n/a	x
n/a	n/a	n/a	x
n/a	n/a	n/a	x
n/a	n/a	n/a	x
n/a	n/a	n/a	x
n/a	n/a	n/a	x
n/a	n/a	n/a	x
n/a	n/a	n/a	n/a
n/a	n/a	n/a	x
n/a	n/a	n/a	x
n/a	n/a	n/a	x
n/a	n/a	n/a	x
n/a	n/a	n/a	x
n/a	n/a	n/a	n/a
n/a	n/a	n/a	x
n/a	n/a	n/a	x
n/a	n/a	n/a	n/a
n/a	n/a	n/a	x
n/a	n/a	n/a	n/a
n/a	n/a	n/a	x
n/a	n/a	n/a	n/a
n/a	n/a	n/a	n/a
n/a	n/a	n/a	x
n/a	n/a	n/a	x
n/a	n/a	n/a	n/a
n/a	n/a	n/a	n/a
n/a	n/a	n/a	n/a
n/a	n/a	n/a	x
n/a	n/a	n/a	x
n/a	n/a	n/a	x
n/a	n/a	n/a	x
n/a	n/a	n/a	x

Source of mean δ18O values
Calculated from data in cited paper or repository
n/a
n/a
x
n/a
n/a
n/a
n/a
n/a
n/a
n/a
n/a
n/a
n/a
n/a
x
x
n/a
n/a
n/a
x
n/a
n/a
n/a
n/a
n/a
n/a
n/a
n/a
n/a
n/a
n/a
n/a
n/a
x
n/a
x
x
x
x
n/a
n/a
n/a
n/a
n/a
n/a
n/a
x
n/a
n/a
x

n/a
n/a
n/a
n/a
x
x
n/a
n/a
n/a
x
n/a
n/a
n/a
x
n/a
x
n/a
n/a
n/a
n/a
x
n/a
x
x
x
x
n/a
x
n/a
n/a
n/a
n/a
n/a
x

Citations (First author, year, DOI/Journal)
Streletskaya, 2015, Earth's Cryosphere
Streletskaya, 2015, Earth's Cryosphere
Vasil'chuk, 2015, Geography Environment Sustainability; Streletskaya, 2015, Earth's Cryosphere
Streletskaya, 2015, Earth's Cryosphere
Vasil'chuk, 2014, 10.1111/bor.12033; Streletskaya, 2015, Earth's Cryosphere
Streletskaya, 2015, Earth's Cryosphere
Vasil'chuk, 2014, 10.1111/bor.12033
Streletskaya, 2015, Earth's Cryosphere
Streletskaya, 2011, 10.1002/ppp.707; Streletskaya, 2015, Earth's Cryosphere
Streletskaya, 2011, 10.1002/ppp.707
Streletskaya, 2011, 10.1002/ppp.707; Streletskaya, 2015, Earth's Cryosphere
Wetterich, 2011, 10.1016/j.quascirev.2011.07.020; Vasil'chuk, 2014, 10.1111/bor.12033; Streletskaya, 2015, E
Wetterich, 2011, 10.1016/j.quascirev.2011.07.020; Streletskaya, 2015, Earth's Cryosphere; Vasil'chuk, 2014, 10
Wetterich, 2011, 10.1016/j.quascirev.2011.07.020; Boereboom, 2013, 10.5194/tc-7-31-2013; Dereviagin, 2013
Vasil'chuk, 2018, 10.1016/j.gsf.2017.04.008
Streletskaya, 2015, Earth's Cryosphere; Opel, 2019, 10.5194/cp-15-1443-2019
Schirrmeister, 2011, 10.1016/j.palaeo.2010.10.045
Schirrmeister, 2011, 10.1016/j.palaeo.2010.10.045; Opel, 2019, 10.5194/cp-15-1443-2019
Vasil'chuk, 2014, 10.1111/bor.12033
Meyer, 2015, 10.1038/NGEO2349
Opel, 2019, 10.5194/cp-15-1443-2019
Opel, 2019, 10.5194/cp-15-1443-2019
Wetterich, 2011, 10.1016/j.quascirev.2011.07.020; Streletskaya, 2015, Earth's Cryosphere; Opel, 2019, 10.519
Opel, 2019, 10.5194/cp-15-1443-2019
Kim, 2019, 10.1002/ppp.1994
Opel, 2019, 10.5194/cp-15-1443-2019
Vasil'chuk, 2014, 10.1111/bor.12033
Schirrmeister, 2017, 10.5194/bg-14-1261-2017; Opel, 2019, 10.5194/cp-15-1443-2019
Vasil'chuk, 2019, 10.1134/S1028334X19050283; Vasil'chuk, 2014, 10.1111/bor.12033; Opel, 2019, 10.5194/cp
Opel, 2019, 10.5194/cp-15-1443-2019; Vasil'chuk, 2017, 10.7256/2453-8922.2017.3.24433
Opel, 2019, 10.5194/cp-15-1443-2019
Opel, 2019, 10.5194/cp-15-1443-2019
Opel, 2019, 10.5194/cp-15-1443-2019
Vasil'chuk, 2018, 10.1134/S1028334X18090192
Opel, 2019, 10.5194/cp-15-1443-2019; Vasil'chuk, 2014, 10.1111/bor.12033
Vasil'chuk, 2018, 10.1134/S1028334X18090192; Streletskaya, 2015, Earth's Cryosphere
Vasil'chuk, 2018, 10.1134/S1028334X18090192
Wetterich, 2011, 10.1016/j.quascirev.2011.07.020; Wetterich, 2014, 10.1016/j.quascirev.2013.11.009; Strelets
Opel, 2011, 10.1002/ppp.667; Streletskaya, 2015, Earth's Cryosphere; Opel, 2017, 10.1177/095968361770222
Opel, 2019, 10.5194/cp-15-1443-2019
Iwahana, 2014, 10.1016/j.polar.2014.01.005
Iwahana, 2014, 10.1016/j.polar.2014.01.005
Vasil'chuk, 2014, 10.1111/bor.12033
Streletskaya, 2015, Earth's Cryosphere
Vasil'chuk, 2014, 10.1111/bor.12033
Murton, 2015, 10.1002/ppp.1843; Vasil'chuk, 2014, 10.1111/bor.12033; Opel, 2019, 10.5194/cp-15-1443-201
Vasil'chuk, 2018, 10.21782/EC2541-9994-2018-5(3-16); Vasil'chuk, 2014, 10.1111/bor.12033; Streletskaya, 20
Vasil'chuk, 2014, 10.1111/bor.12033
Wetterich, 2018, 10.1002/ppp.1979
Vasil'chuk, 2018, 10.7256/2453-8922.2018.3.27121

Streletskaya, 2015, Earth's Cryosphere
Vasil'chuk, 2014, 10.1111/bor.12033
Streletskaya, 2015, Earth's Cryosphere
Streletskaya, 2015, Earth's Cryosphere
Vasil'chuk, 2018, 10.3103/S0145875218010131; Vasil'chuk, 2014, 10.1111/bor.12033
Vasil'chuk, 2017, 10.21782/EC1560-7496-2017-5(24-35); Vasil'chuk, 2014, 10.1111/bor.12033
Vasil'chuk, 2018, 10.1002/ppp.1991
Vasil'chuk, 2018, 10.1002/ppp.1991
Vasil'chuk, 2018, 10.1002/ppp.1991
Vasil'chuk, 2015, GEOGRAPHY ENVIRONMENT SUSTAINABILITY; Streletskaya, 2015, Earth's Cryosphere
Wetterich, 2019, 10.5194/bg-16-4261-2019
Yang, 2011, 10.1007/s11430-010-4029-5
Brosius, 2012, 10.1029/2011JG001810
Meyer, 2010, 10.1029/2009GL041013; Meyer, 2010, 10.1016/j.quascirev.2010.08.005; Iizuka, 2019, 10.1016/j
Lapointe, 2017, 10.1016/j.palaeo.2017.08.006
Kanevskiy, 2017, 10.1016/j.geomorph.2017.09.001
Schirrmeister, 2016, 10.1016/j.quascirev.2016.02.009; St-Jean, 2011, 10.1002/ppp.680
Brosius, 2012, 10.1029/2011JG001810
Lachniet, 2012, 10.1016/j.yqres.2012.05.007; Lachniet, 2016, 10.1002/2016WR019436
Fritz, 2012, 10.1016/j.palaeo.2011.12.015
St-Jean, 2011, 10.1002/ppp.680
Calmels, 2012, 10.1139/E2012-023; Porter, 2016, 10.1016/j.quascirev.2016.02.006
Fritz, 2015, 10.5194/tc-9-737-2015
Fritz, 2015, 10.5194/tc-9-737-2015
Fritz, 2012, 10.1016/j.palaeo.2011.12.015; Fritz, 2016, 10.1016/j.quascirev.2016.02.00
St-Jean, 2011, 10.1002/ppp.680; Grinter, 2018, 10.1017/qua.2018.65
Porter, 2019, 10.1038/s41467-019-09622-y
Michel, 2011, 10.1002/ppp.721
Lacelle, 2014, 10.1016/j.chemgeo.2014.01.005
Holland, 2019, under review
Holland, 2019, under review
Holland, 2019, under review
Holland, 2019, under review
Coulombe, 2019, 10.5194/tc-13-97-2019